

Fluvial landscapes of the Harappan civilization

Liviu Giosan^{a,1}, Peter D. Clift^{b,2}, Mark G. Macklin^c, Dorian Q. Fuller^d, Stefan Constantinescu^e, Julie A. Durcan^c, Thomas Stevens^f, Geoff A. T. Duller^c, Ali R. Tabrez^g, Kavita Gangal^h, Ronojoy Adhikariⁱ, Anwar Alizai^b, Florin Filip^e, Sam VanLanhingham^j, and James P. M. Syvitski^k

^aGeology and Geophysics, Woods Hole Oceanographic Institution, Woods Hole, MA 02543; ^bSchool of Geosciences, University of Aberdeen, Aberdeen AB24 3UE, United Kingdom; ^cInstitute of Geography and Earth Sciences, Aberystwyth University, Aberystwyth SY23 3DB, United Kingdom; ^dInstitute of Archaeology, University College London, London WC1H 0PY, United Kingdom; ^eDepartment of Geography, University of Bucharest, Bucharest, 70709, Romania; ^fDepartment of Geography, Royal Holloway, University of London, Egham, Surrey TW20 0EX, United Kingdom; ^gNational Institute of Oceanography, Karachi, 75600, Pakistan; ^hSchool of Mathematics and Statistics, Newcastle University, Newcastle upon Tyne NE1 7RU, United Kingdom; ⁱThe Institute of Mathematical Sciences, Chennai 600 113, India; ^jSchool of Fisheries and Ocean Sciences, University of Alaska, Fairbanks, AK 99775-7220; and ^kCommunity Surface Dynamics Modeling System (CSDMS) Integration Facility, Institute of Arctic and Alpine Research (INSTAAR), University of Colorado, Boulder, CO 80309-0545

Edited by Charles S. Spencer, American Museum of Natural History, New York, NY, and approved March 20, 2012 (received for review August 5, 2011)

The collapse of the Bronze Age Harappan, one of the earliest urban civilizations, remains an enigma. Urbanism flourished in the western region of the Indo-Gangetic Plain for approximately 600 y, but since approximately 3,900 y ago, the total settled area and settlement sizes declined, many sites were abandoned, and a significant shift in site numbers and density towards the east is recorded. We report morphologic and chronologic evidence indicating that fluvial landscapes in Harappan territory became remarkably stable during the late Holocene as aridification intensified in the region after approximately 5,000 BP. Upstream on the alluvial plain, the large Himalayan rivers in Punjab stopped incising, while downstream, sedimentation slowed on the distinctive mega-fluvial ridge, which the Indus built in Sindh. This fluvial quiescence suggests a gradual decrease in flood intensity that probably stimulated intensive agriculture initially and encouraged urbanization around 4,500 BP. However, further decline in monsoon precipitation led to conditions adverse to both inundation- and rain-based farming. Contrary to earlier assumptions that a large glacier-fed Himalayan river, identified by some with the mythical Sarasvati, watered the Harappan heartland on the interfluve between the Indus and Ganges basins, we show that only monsoonal-fed rivers were active there during the Holocene. As the monsoon weakened, monsoonal rivers gradually dried or became seasonal, affecting habitability along their courses. Hydroclimatic stress increased the vulnerability of agricultural production supporting Harappan urbanism, leading to settlement downsizing, diversification of crops, and a drastic increase in settlements in the moister monsoon regions of the upper Punjab, Haryana, and Uttar Pradesh.

Indus Valley | floods | droughts | climate change | archaeology

The Harappan or Indus Civilization (1–8) developed at the arid outer edge of the monsoonal rain belt (9, Fig. 1) and largely depended on river water for agriculture (10). The Harappans settled the Indus plain over a territory larger than the contemporary extent of Egypt and Mesopotamia combined (Figs. 2 and 3). Between the Indus and Ganges watersheds, a now largely defunct smaller drainage system, the Ghaggar-Hakra, was also heavily populated during Harappan times (4, 5). Controlled by the Indian monsoon and the melting of Himalayan snow and glaciers (2, 11, 12), the highly variable hydrologic regime, with recurring droughts and floods, must have been a critical concern for Harappans, as it is today for almost a billion people living on the Indo-Gangetic Plain in Pakistan, northern India, and Bangladesh. In such challenging environmental conditions, both the development and the decline of the Harappan remain equally puzzling (13). We investigate how climate change affected this civilization by focusing on fluvial morphodynamics, which constitutes a critical gap in our current understanding of the Harappan in the way it affects habitability and human settlement patterns near rivers in arid regions.

Brief Harappan History

The Harappan cultural tradition (2–4) evolved during an Early Phase (5,200–4,500 y ago) from antecedent agricultural communities of the hills bordering the Indus alluvial plain to the west and reached its urban peak (Mature Phase) between approximately 4,500 and 3,900 y ago. The Harappans were agrarian but developed large, architecturally complex urban centers and a sophisticated material culture coupled with a robust trade system. In contrast to the neighboring hydraulic civilization of Mesopotamia (14) and to Egypt (15), Harappans did not attempt to control water resources by large-scale canal irrigation (16). Deurbanization ensued after approximately 3,900 y ago and was characterized by the development of increasingly regional artifact styles and trading networks as well as the disappearance of the distinctive Harappan script (2–4; 17). While this is often referred to as “collapse,” archaeological evidence indicates a protracted and regionally varied process (2, 4, 17). Many settlements exhibit continuity, albeit with reduced size, whereas many other riverine sites are abandoned, especially along the lower Indus and the Ghaggar-Hakra course (3–5; *SI Text*). Between 3,900 and 3,000 y ago, there was a proliferation of smaller, village-type settlements (2–4, 6, 18), especially in the Himalayan foothills and the western part of the Ganges basin along the Yamuna River and on the Yamuna-Ganga interfluve (Fig. 3B).

Socio-economic theories have been invoked to address the collapse of urban Harappan society, including foreign invasions, social instabilities, and decline in trade (4). Alternatively, environmental factors were suggested to play a decisive role in the decline (1, 2, 8); among these, regional aridification, hydrological changes such as the drying or capture of the Ghaggar-Hakra system (3, 4, 7, 19, 20), as well as human-induced environmental degradation (21) have been advanced. Despite almost a century of research, a clear perspective on the role played by fluvial dynamics in influencing the fate of the Harappan civilization has been hampered by a lack of high-resolution topographic data and sedimentary chronologies. Shuttle Radar Topography Mission (SRTM) data (22) combined with field surveys and radiocarbon and optically stimulated luminescence dating offer us a way to

Author contributions: L.G., P.D.C., M.G.M., and D.Q.F. designed research; L.G., P.D.C., M.G.M., D.Q.F., S.C., J.A.D., T.S., G.A.T.D., A.R.T., K.G., R.A., A.A., F.F., S.V., and J.P.M.S. performed research; L.G., P.D.C., M.G.M., D.Q.F., S.C., J.A.D., T.S., G.A.T.D., A.R.T., K.G., R.A., and J.P.M.S. analyzed data; and L.G. and D.Q.F. wrote the paper.

The authors declare no conflict of interest.

This article is a PNAS Direct Submission.

¹To whom correspondence should be addressed. E-mail: lgiosan@whoi.edu.

²Present address: Department of Geology and Geophysics, Louisiana State University, Baton Rouge, LA 70803.

See Author Summary on page 10138 (volume 109, number 26).

This article contains supporting information online at www.pnas.org/lookup/suppl/doi:10.1073/pnas.1112743109/DCSupplemental.

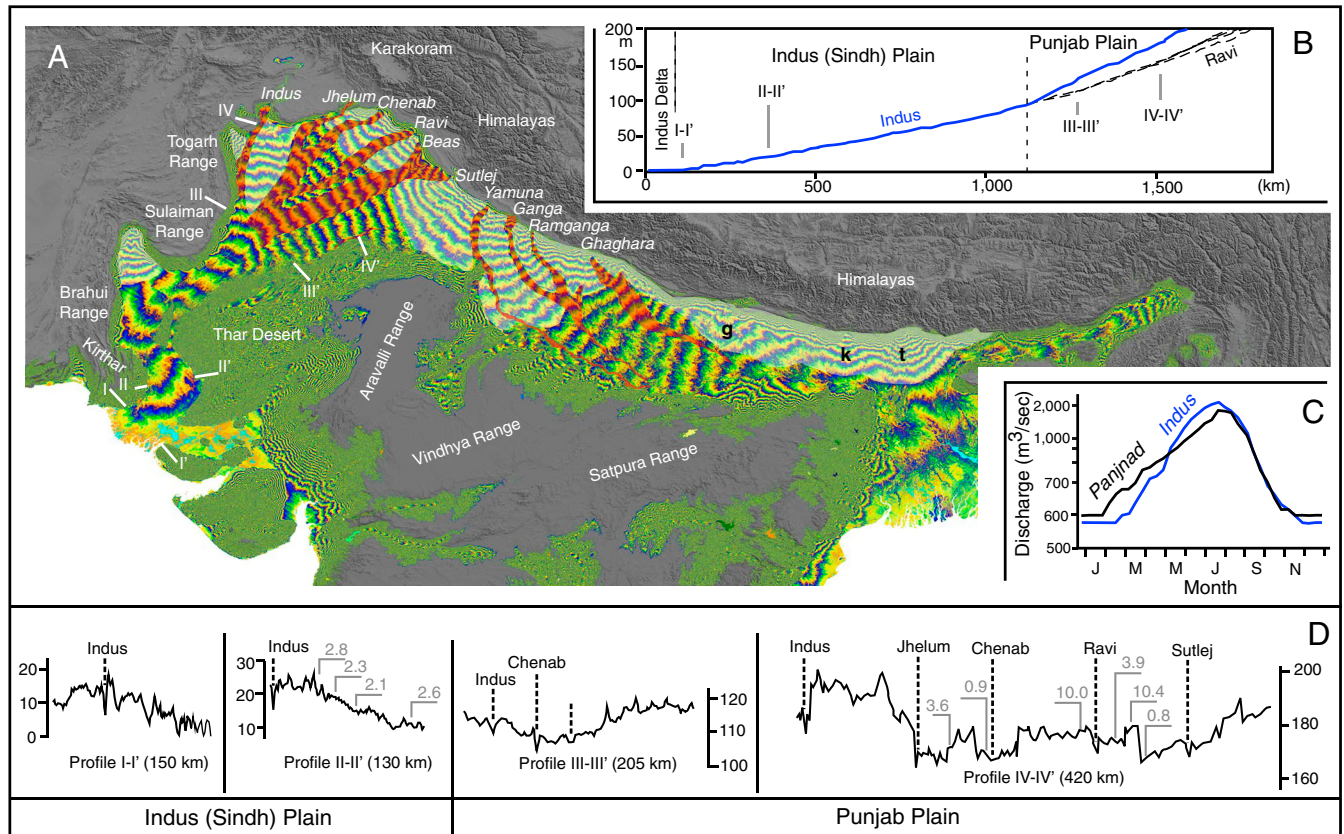


Fig. 1. Large-scale morphology of the Indo-Gangetic Plain (for altitudes, pattern of colors repeats every 10 m to 300 m in height; higher landscape in gray). Convex downslope, aggradational landscapes (e.g., Tista = *t*; Kosi = *k*; Gandak = *g*) have a lighter mask, whereas incisional landscapes have a red mask. (*B*) Along-channel longitudinal profiles for the Indus and its Punjab tributaries. (*C*) Hydrographs for the Indus and confluent Punjab tributaries (Panjnad River). (*D*) Profiles across the extended Indus plain (in meters above sea level). River channel locations are identified on the profiles, as are locations and ages of studied fluvial sedimentary deposits in Sindh and Punjab (ages in thousands of years).

analyze fluvial landforms and date deposits of the Indo-Gangetic Plain. In this context, we reexamine archaeological site distribution to understand how climate-controlled changes in river dynamics affected the Harappans (*SI Text*).

Morphodynamics of the Indo-Gangetic Plain

The Indo-Gangetic Plain (Fig. 1) was built during the Cenozoic with sediments derived primarily from the Himalayas (23). Our digital elevation model shows a trend from aggradation in the eastern part of the Indo-Gangetic Plain toward incising rivers in the west (24), probably driven by the westward weakening of the monsoonal rains along the Himalayas (9, 25). In the eastern Indo-Gangetic Plain, alluvial megafans were actively built during the Holocene by rivers with large, highly seasonal sediment discharge and low stream power (25). In contrast, rivers in the western Indo-Gangetic Plain (Fig. 1) are largely degradational after emerging from the Himalayan foothills. Wide, shallowly incised valleys separated by interfluvia characterize the Indus and its tributaries in Punjab (26) as well as the Ganges and its westernmost tributaries (Fig. 1).

The Old Beas Survey (2, 27; 28) previously documented incision of the terminal Pleistocene sediments on the Beas-Ravi interfluvia at and near Harappa followed by stable conditions and occupation levels after approximately 7,700 y ago. On the interfluvia in Punjab, we dated the latest fluvial channel deposits to approximately 10,000 y ago (Fig. 2B; *SI Text*), confirming that large-scale fluvial sedimentation ceased at the beginning of the Holocene. Within the entrenched river valleys, we mapped abandoned river channel belts and terraces (26), which indicate periodic but progressive incision (29, 30). Our dates on incised valley deposits vary in age between 700 and 3,900 y (Fig. 2B; *SI Text*).

Thus, rivers in Punjab started to incise after 10,000 y ago, but before 3,900 y ago. As documented along the Himalayan course of the Sutlej River (12), the eastermost tributary of the Indus, century-long phases of sediment load decline caused by weak monsoons were responsible for incision, primarily in the early Holocene between approximately 10,000 and 8,700 y ago. The presence of Harappan and even earlier settlements within these incised valleys (*vide infra*) also argues for major incision predating the Harappan. During Harappan times, the alluvial landscape in Punjab offered suitable terrain for floodwater farming within incised valleys and important protection against large floods on interfluvia.

The similarity of incision profiles (29, 31) for Indus tributaries across Punjab (Fig. 1) reflects comparable hydrological histories during the Holocene (25). On the other hand, high water discharge and sediment load (29) explain the relatively steep longitudinal profile of the Indus. We note the sharp contrast between the degradational character of the tributaries of the Indus and the Ganges in the western Indo-Gangetic Plain and the lack of wide incision valleys along the Ghaggar-Hakra interfluvia (Figs. 1 and 24). Numerous speculations have advanced the idea that the Ghaggar-Hakra fluvial system, at times identified with the lost mythical river of Sarasvati (e.g., 4, 5, 7, 19), was a large glacier-fed Himalayan river. Potential sources for this river include the Yamuna River, the Sutlej River, or both rivers. However, the lack of large-scale incision on the interfluvia demonstrates that large, glacier-fed rivers did not flow across the Ghaggar-Hakra region during the Holocene. Existing chronologies (27, 28) and our own age on the bank of Sutlej (*SI Text*) identified deposits of Late Pleistocene age, indicating that the interfluvia formed instead

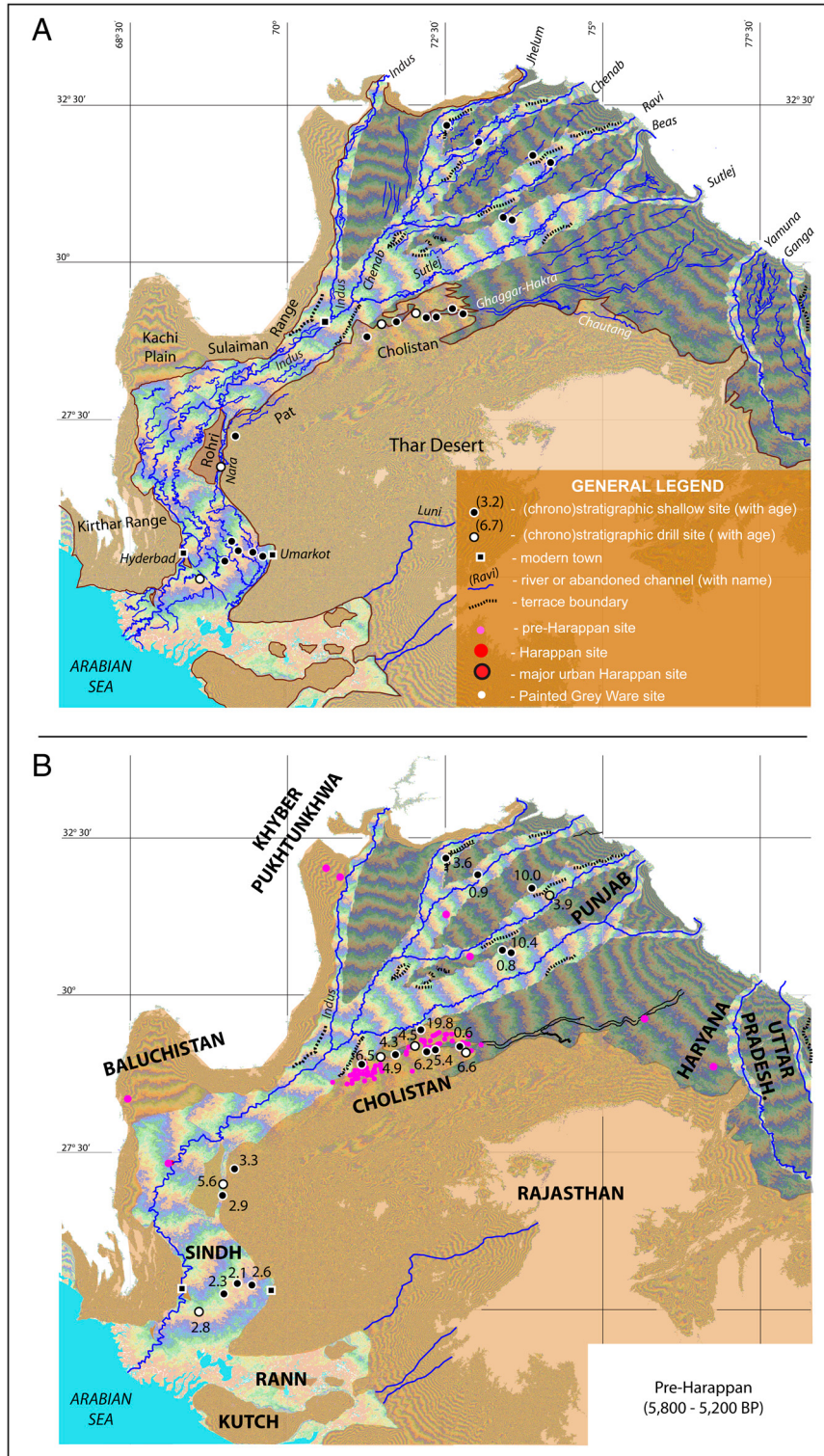


Fig. 2. (A) Morphology of the western Indo-Gangetic plain with interfluves (in gray mask), incised valleys (no mask), terrace edges (as dashed black lines), and active and fossilized river channels (in blue). Legend further indicates sampling locations and types. (B) Pre-Harappan sites with modern region names, chronological information (youngest fluvial deposits at all sites), and selected town names.

during the last glacial period. Provenance detection (32) suggests that the Yamuna may have contributed sediment to this region during the last glacial period, but switched to the Ganges basin before Harappan times.

The present Ghaggar-Hakra valley and its tributary rivers are currently dry or have seasonal flows. Yet rivers were undoubtedly active in this region during the Urban Harappan Phase. We recovered sandy fluvial deposits approximately 5,400 y old at Fort Abbas in Pakistan (*SI Text*), and recent work (33) on the upper Ghaggar-Hakra interfluvium in India also documented Holocene

channel sands that are approximately 4,300 y old. On the upper interfluvium, fine-grained floodplain deposition continued until the end of the Late Harappan Phase, as recent as 2,900 y ago (33) (Fig. 2B). This widespread fluvial redistribution of sediment suggests that reliable monsoon rains were able to sustain perennial rivers earlier during the Holocene and explains why Harappan settlements flourished along the entire Ghaggar-Hakra system without access to a glacier-fed river (5, Fig. 34). Similar, strictly monsoonal rivers maintaining a groundwater-fed base flow are now active only on the more humid Ganga basin

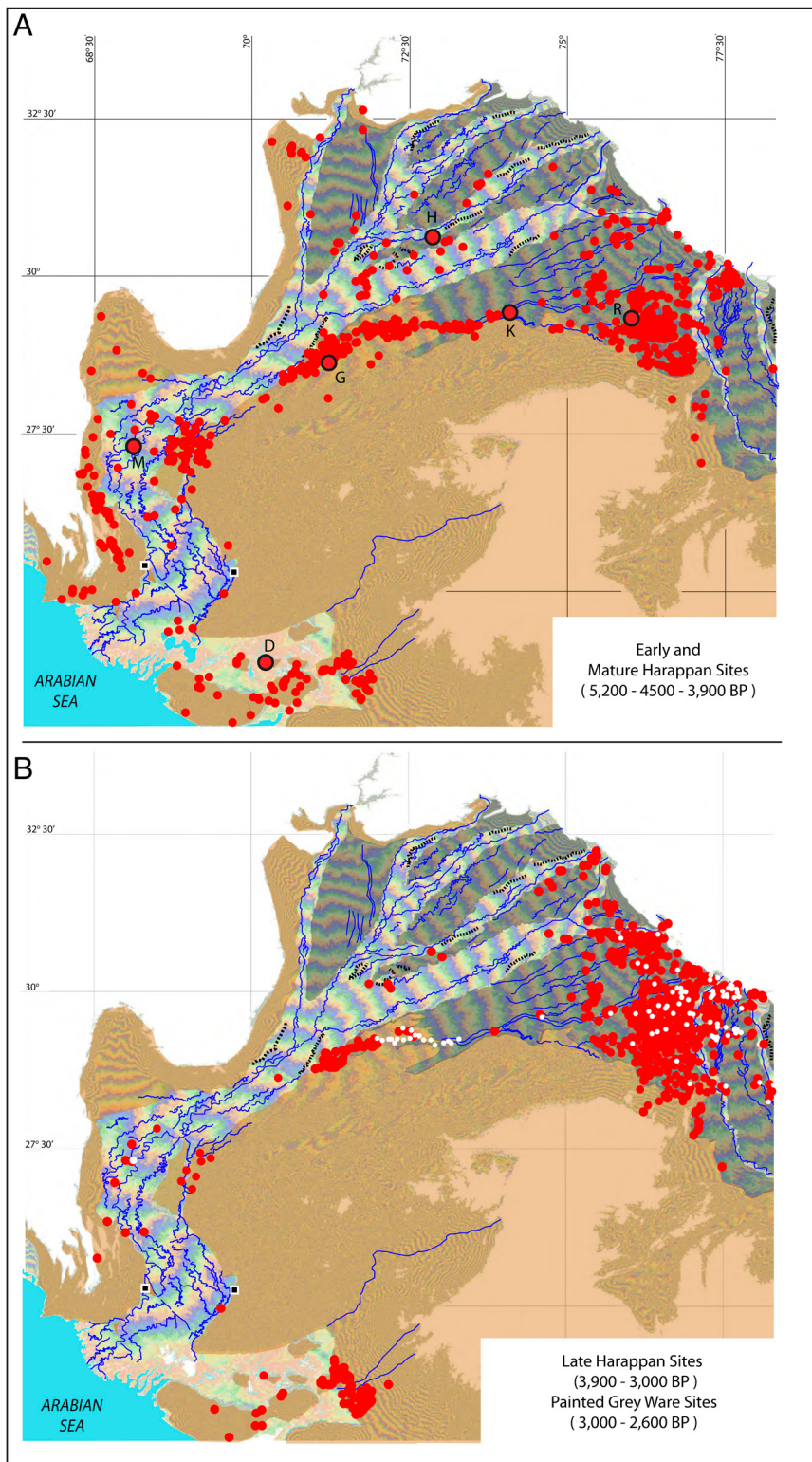


Fig. 3. Settlements on morphological units of the western Indo-Gangetic plain (see Fig. 2 for color conventions and legend). (A) Early and Mature Harappan sites, with names of some major urban centers: *D* = Dholavira; *M* = Mohenjo-Daro; *G* = Ganweriwala; *H* = Harappa; *K* = Kalibangan; *R* = Rakhigarhi. (B) Late Harappan (red) and Painted Gray Ware (white) sites.

(34). We also document renewed fluvial deposition on the lower Ghaggar-Hakra system approximately 700 y ago, which indicates that seasonal monsoon flows intensified episodically during the late Holocene and may provide an explanation for the high concentration of medieval fortified sites in this region (5).

Farther to the south, the five Punjab tributaries of the Indus merge to form the Panjnad River, before joining the Indus (Figs. 1 and 24). Incision (4–5 m deep) between the two confluences and further south along the greater Indus separates vertically the

modern floodplain and the southernmost extension of the Ghaggar-Hakra interfluvia in the Cholistan region. Dunes younger than 1,500 y old on the edge of the expanding Thar Desert have begun to cover this region of the interfluvia, but sediment originating from the Indus-Punjab system, the Ghaggar-Hakra, or from both of these river systems was deposited as late as 4,250 y ago (Fig. 2B; *SI Text*). Zircon dating of sand in this confluence region indicates inputs from both Beas and Sutlej drainage basins (32). Continuing to the southwest on the Ghaggar-Hakra interfluvia, we

document well-watered lands in the region of Pat, where channels ran parallel with the Indus and joined the Nara valley; their fluvial deposits at Fakirabad, among the dunes of the expanding desert, are even younger at approximately 3,350 y old. Further south, the Nara valley, which would be currently dry if not for modern irrigation, also had active fluvial sedimentation approximately 2,900 y ago (Fig. 2B; *SI Text*).

Downstream in the province of Sindh, the Indus River built a unique distributive-type fluvial system that we term the Indus fluvial mega-ridge (Fig. 1). The alluvial plain here is convex up (35–37), showing maximum aggradation near the modern channel belt and tapering out toward the plain edges (*SI Text*). The cross-sectional relief of the ridge is very subdued (over 100 km wide and 10–15 m high; Fig. 1) and the river is stable on its apex because the thalweg is incised as deep as the ridge. Fossil channel belts and associated crevasse splays occur on both sides of the modern Indus course (Fig. 2A; *SI Text*). Radiocarbon-dated fluvial deposits of old channel belts in lower Sindh indicate that aggradation was minimal during the late Holocene (between 2.4 m/kyr near the mega-ridge top down to less than 1 m/kyr near its edge; Fig. 2B; *SI Text*). This relative stability of the late Holocene landscape suggests that large avulsions of the Indus were rare and distributary channels acted mainly as overspills, as documented for the historical period (38, 39). In contrast, at our Matli floodplain drill site on top of the Indus mega-ridge (Fig. 2B; *SI Text*), sedimentation rates were at least three times higher between approximately 7,200 and 2,700 y ago compared to the last approximately 2,700.

We speculate that the development of the Indus fluvial mega-ridge was also the direct consequence of late Holocene aridity (12, 40–42). Hydroclimate in the western Indo-Gangetic Plain is influenced by both the Indian summer monsoon system and westerly winter disturbances bringing humidity from the Mediterranean, Black, and Caspian Seas (9, 11). Most sediment is delivered to the Indus by floods after high-intensity monsoon storms (43), but the bulk of Indus water discharge is dependent on snow melt (11). The weakening of the monsoon after approximately 5,000 y ago compared to the slower decline in winter precipitation originating in western Asia (40, 42, 44, Fig. 4) must have resulted in a reduction in sediment load compared to water discharge, causing channel incision and stabilization (12; *SI Text*) and leading to longer intervals of decoupling between channels and the alluvial plain. The subdued relief of the fluvial ridge, resulting from less frequent breaches and overspills as well as cohesive banks (35), which are typical for arid regions, are not favorable to avulsions. Rarity of large scale avulsions reinforces deposition close to existing channel belts and allows for the slow growth of the mega-ridge. Within the deep active channels on top of the ridge, effective conveyance of sediments toward the coast for the build-up of a new deltaic depocenter in western lower Sindh (45, 46) must have diverted most of the sediment away from the Indus alluvial plain in the late Holocene.

Our analysis reveals a palimpsest of fluvial forms and deposits in the western region of the Indo-Gangetic Plain; however, one constant trait that is evident across the entire Harappan landscape is the change from a more energetic fluvial regime earlier in the Holocene (before approximately 5,000 y ago; Fig. 4) to increased stability of alluvial forms by Early Harappan times, and even drying up of some river channels during and after Harappan times.

Settlement Dynamics in the Harappan Domain

The distribution of Harappan sites within the incised valleys of Punjab (Fig. 3A) provides clear evidence that rivers were already entrenched by 5,200 y ago or earlier (Fig. 2B). Numerous sites are present in the incised valley at the confluence zone of the Indus with the Punjab rivers. In this region of confluences, regardless of their past geometries, backwater flooding would have

been common because the Indus and its tributaries in Punjab reach their flood stages asynchronously (Fig. 1). Settlements on the Punjab interfluvia, including Harappa, also tend to be located near their edges, close to the fertile, annually flooded areas in the incised valleys (Fig. 3A; 28). Farther to the east, Harappan sites have been reported along a network of smaller monsoon-fed rivers in the upper region of the Ghaggar-Hakra domain (i.e., Haryana and upper Punjab; 19, 47, 48) as well as along and within the incised valley of the Yamuna and the Yamuna-Ganga interfluvia (49, 50). As the climate continued to become drier during late Harappan times (Fig. 4), the number of sites increased in the upper Punjab and Haryana, especially on interfluvia near the Himalayan piedmont where monsoonal rains are more consistent (Fig. 3B).

The largest agglomeration of mature Harappan sites, including the urban Ganweriwala, occurs on the lowermost Ghaggar-Hakra interfluvia (5, 49) in modern Cholistan. The proximity to both the Ghaggar-Hakra valley and the well-watered Indus-Punjab river confluence region provides the best explanation for the unusual continuity and high-density occupation of the lower Ghaggar-Hakra interfluvia (Figs. 2 and 3). Recent Harappan discoveries in the Thar Desert adjacent and along the Nara valley (51) support our reconstructions of a better-watered past for this dry region as well. As channels of the Ghaggar-Hakra dried through the Late Harappan Phase, fewer sites occur on the lower part of the Sutlej-Yamuna interfluvia (4, 5), with the notable exception of sites closest to the Indus where access to water remained somewhat reliable (Fig. 3B). In contrast, the number of sites in the upper region of the interfluvia increased as they did beyond the Yamuna to the east (4, 18, 50; *SI Text*, Fig. 3B). Later, Painted Gray Ware sites were reestablished along the middle Ghaggar-Hakra course (Fig. 3B), suggesting a possible reinvigoration of seasonal river flows during the Iron Age (5). The lack of Painted Gray Ware sites at the distal end of the Ghaggar-Hakra system (4, 5), however, supports our chronostratigraphic evidence that river flow had become ephemeral and did not reach as far as the Indus.

In Sindh, in the southern part of the Harappan domain, many archaeological sites are found on landforms that were not affected by fluvial erosion or deposition, such as the western Pakistan ranges and bedrock inselbergs raised above the alluvial plain. However, in upper Sindh, good preservation of early and mature Harappan sites on the alluvial plain (45), including Mohenjo-Daro, suggests that the Indus mega-ridge has been relatively stable in that region since Harappan times. In contrast, in lower Sindh, just a few Harappan sites have been discovered on the eastern delta plain (52), supporting the idea of a switch of the fluvio-deltaic depocenter to the west (45, Figs. 2 and 3). Any settlement on the alluvial plain that may have existed in the southwestern part of Sindh is probably buried under later fluvial sediments. Sites in Kutch, a coastal region that was never dependent on flood agriculture but instead relied on trade, remained active into late Harappan times (4, Fig. 3B), when settlements were far fewer on the Indus plain.

Although erosion or burial of archaeological sites is an important process in fluvial environments, preservation of Harappan archaeological sites in potentially dynamic contexts such as entrenched valleys, river confluences, and accretionary distributive fluvial forms indicates relatively low fluvial activity across the wider alluvial plain since the time settlements were established. In this context, however, the preferential occurrence of Harappan urban sites on interfluvia, but in close proximity to floodable, agriculturally viable land (20, 24), suggests awareness of devastating floods that can occur on Himalayan rivers. Settling of the Ghaggar-Hakra river system is the best example of an adaptation strategy that takes advantage of smaller floods along monsoonal rivers, where monsoon rains are not augmented by meltwater. However, most floods, whether in entrenched valleys in Punjab, along overspills in Sindh, or along the smaller rivers of the Ghaggar-Hakra system, must have been predominantly benign

in character to be able to foster intensive agriculture and also regular enough not to require canal irrigation.

Diminished monsoon rains and less reliable flooding during late Harappan times could explain the expansion of settlements near the headwaters of the Ghaggar-Hakra system, where small-scale floods probably remained more dependable and where rains allowed summer-cropping on interfluviums. Agriculture, land development, and continuous habitation can skew the distribution of archaeological sites, but such biases should be minimal in desert areas like Cholistan. In upper Punjab, Haryana, and Uttar Pradesh, where historical and modern destruction of sites has been intensive, the increase in the number of sites during the late Harappan shows an unambiguous trend. In contrast, in lower Punjab and Sindh, regions of similarly intense history of human activities, the number of sites decreased over the same interval.

Climate Change and the Harappans

For the arid Indus region, river floods have always been far more important and reliable for agriculture than rainfall. As during the Harappan era (7, 10, 20), inundation agriculture during the *Rabi* season (winter crops) was dominant along the Indus and its tributaries (10, 38, *SI Text*) prior to the development of the largest irrigation system in the world in 20th century Pakistan. Hydroclimate reconstructions for South and Central Asia (39–41) show that precipitation from both monsoon and westerly sources that feed rivers of the western Indo-Gangetic Plain (20) decreased since approximately 5,000 y ago, and was at its lowest after approximately 4,000 y BP (Fig. 4). This drying of the Indus region supports the hypothesis that adaptation to aridity contributed to social complexity and urbanization (1, 52). An intense drought period around 4,200 y ago, linked to major disruptions in Egypt and Mesopotamia (53–56), coincides instead with the flourishing of Harappan urbanism within the limits of available chronology. This event, recorded

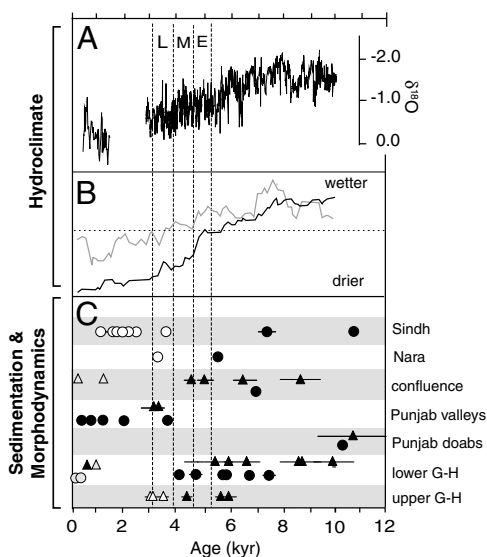


Fig. 4. Palaeo-hydroclimate reconstructions and sedimentary activity chronology for the Harappan domain. (A) Indian monsoon precipitation reconstruction (35). (B) Synthetic reconstructions for the Indian monsoon domain (black) and westerly precipitation (37) (gray). (C) Sedimentation ages for fluvial forms in: Sindh (i.e., Indus fluvial mega-ridge); Nara Valley; Indus-Panjab-Ghaggar-Hakra confluence; Punjab incised valleys; Punjab interfluviums (doabs); and the lower and upper Ghaggar-Hakra (G-H) system regions, respectively. OSL dates are represented by triangles and calibrated AMS radiocarbon dates by circles; error bars are shown if larger than the symbol size. Fluvial deposits are shown in black- and white-filled symbols (for high vs. low sedimentation rate deposits, respectively), whereas dunes are represented by gray-filled symbols. Ages for the upper Ghaggar-Hakra system are from Saini et al. (33). The temporal extent of each Harappan phase is indicated by vertical dashed lines (*E* = early; *M* = mature; *L* = late).

at the start of the aridification process in South Asia, had affected the total Indus discharge (57), but aridification may have diminished the intensity of floods and allowed inundation agriculture to expand along the Indus and its tributaries (20). However, our analysis of fluvial landscapes suggests that further drying was detrimental for the Harappans, who relied on annual floods to sustain their economy. Good preservation of numerous archaeological sites at locations seemingly vulnerable to flooding, erosion, or burial suggest that, as aridity intensified, monsoon-augmented floods became less frequent and/or less intense. The most spectacular case of climate-controlled landscape transformation is the Ghaggar-Hakra system, which became ephemeral and was largely abandoned.

Settlements of the posturban period are preferentially located near the easily flooded region at the confluence of the Indus with rivers in Punjab or in eastern regions with more reliable monsoon rains. Diversification of agriculture towards *Kharif* (summer) rain-based crops and the increase in drought-tolerant crops like millets (*SI Text*) at the end of the urban phase (58) reveal intense efforts to adapt to hydroclimatic stress at the arid outer edge of the monsoonal rain belt. The climate-controlled decline in floods concurrent with the reduction of monsoon rains probably led to a decrease in surpluses for supporting that part of the population that was not involved directly in agriculture, which in turn led to diminished social complexity. Although snowmelt continued to regularly provide water to the Indus and its Himalayan tributaries (57), the Harappans did not develop canal irrigation. In contrast to inhabitants of Mesopotamia and Egypt, which were surrounded by arid lands, the Harappans had the option to migrate east toward more humid regions of the Indo-Gangetic Plain. Migration toward the periphery could have contributed to reduced population in the core region of the Harappan domain and the decline of urban centers. The unprecedented scale of hydroclimatic stresses must have increased the vulnerability of Harappan society, but does not provide a simple, deterministic explanation for the transformations in site size, distribution, and interrelationships across the whole civilization area (2, 4, 6, 17, 59). The longevity of the decentralized late Harappan phase and continued habitation documented in places in Sindh and lower Punjab suggests that the perennial flows of the Indus and its Himalayan tributaries still flooded agriculturally viable lands, albeit less extensively than earlier. As a lesson from the past, the possible return to stronger monsoon-augmented floods (60), similar to the disastrous events of 2010 in Pakistan, may render current flood controls and irrigation systems vulnerable and require the large-scale adaptation of modern society in the western Indo-Gangetic Plain.

Methods

We used SRTM (22) data to map the Indo-Gangetic Plain, focusing on its western region (see *SI Text* for full methods). We identified active and abandoned river courses, incised valleys and interfluviums, terraces, fluvial ridges, alluvial fans, piedmonts, and dune fields. To avoid misinterpreting the morphology due to post-Harappan alterations of the Indo-Gangetic Plain via natural and anthropogenic processes, especially over the past century, we only interpreted features that retain a clear, large-scale SRTM topographical expression. Using SRTM-based digital elevation models, satellite photography, and geological maps, we selected key locations in Sindh and Punjab (Pakistan) to investigate the stratigraphy of the uppermost Indo-Gangetic Plain fill. Chronologies for fluvial and aeolian deposits in newly collected cores, trenches, and large-scale exposures in sand quarries were constructed based on accelerator mass spectrometry (AMS) radiocarbon and optically stimulated luminescence dating (*SI Text*). Location and age estimates of archaeological sites (*SI Text*) provided additional chronological information to assess the dynamics of fluvial environments.

ACKNOWLEDGMENTS. We thank the personnel and Dr. M.M. Rabbani, then Director General of the National Institute of Oceanography in Karachi, for logistical support in Pakistan. We thank Dr. Rita Wright for sharing information on sites of the Harappa and Lower Beas Regional Survey. This study was supported by grants from the National Science Foundation, the Leverhulme Trust, Woods Hole Oceanographic Institution, the University of Aberdeen, and Louisiana State University.

1. Madella M, Fuller DQ (2006) Palaeoecology and the Harappan Civilisation of South Asia: a reconsideration. *Quaternary Sci Rev* 25:1283–1301.
2. Wright RP (2010) *The Ancient Indus: Urbanism, Economy and Society* (Cambridge, Cambridge University Press).
3. Kenoyer JM (1998) *Ancient Cities of the Indus Valley Civilization* (Oxford University Press, Oxford).
4. Possehl GL (2002) *The Indus Civilization: A Contemporary Perspective* (Altamira Press, Lanham, MD).
5. Mughal MR (1997) *Ancient Cholistan: Archaeology and Architecture* (Ferozsons, Lahore).
6. Gangal K, Vahia M, Adhikari R (2010) Spatio-temporal analysis of the Indus urbanization. *Current Sci India* 98:846–852.
7. Fuller DQ, Madella M (2002) *Indian Archaeology in Retrospect. Protohistory*, eds S Settar and R Korisettar (Manohar Publishers, New Delhi), vol. II, pp 317–390.
8. MacDonald G (2011) Potential influence of the Pacific Ocean on the Indian summer monsoon and Harappan decline. *Quatern Int* 299:140–148.
9. Bookhagen B, Burbank DW (2010) Towards a complete Himalayan hydrological budget: the spatiotemporal distribution of snow melt and rainfall and their impact on river discharge. *J Geophys Res* 115:F03019.
10. Miller M-LH (2006) *Agriculture and Irrigation in Archaeology*, eds C Stanish and J Marcus (Cotsen Institute of Archaeology Press, Los Angeles), pp 92–128.
11. Karim A, Veizer J (2002) Water balance of the Indus river basin and moisture source in the Karakoram and western Himalayas: implications from hydrogen and oxygen isotopes river water. *J Geophys Res* 107:4362, doi: 10.1029/2000JD000253.
12. Bookhagen B, Fleitmann D, Nishiizumi K, Strecker MR, Thiede RC (2006) Holocene monsoonal dynamics and fluvial terrace formation in the northwest Himalaya, India. *Geology* 34:601–604.
13. Lawler A (2008) Unmasking the Indus. *Science* 320:1276–1285.
14. Adams RM (1981) *Heartland of Cities: Surveys of Ancient Settlement and Land Use on the Central Floodplain of the Euphrates* (University of Chicago Press, Chicago).
15. Butzer KW (1976) *Early Hydraulic Civilization in Egypt: A Study in Cultural Ecology* (University of Chicago Press, Chicago).
16. Schumm SA (2007) *River Variability and Complexity* (Cambridge University Press, Cambridge).
17. Kenoyer JM (2006) *Historical Roots in the Making of 'the Aryan'*, ed R Thapar (National Book Trust, New Delhi), pp 41–97.
18. Kumar M (2009) *Linguistics, Archaeology and the Human Past, Occasional Paper 7*, eds T Osada and A Uesugi (Research Institute for Humanity and Nature, Nakanishi Printing Co. Ltd, Kyoto), pp 1–75.
19. Radhakrishna BP, Merh SS (1999) *Vedic Saraswati, Memoir*, (Geological Society of India, India), Vol. 42.
20. Wright RP, Bryson R, Schuldenrein J (2008) Water supply and history: Harappa and the Beas regional survey. *Antiquity* 82:37–48.
21. Fairservis WA (1967) The origins, character and decline of an early civilization. *Am Mus Novit* 2302:1–48.
22. Farr TG, et al. (2007) The Shuttle Radar Topography Mission. *Rev Geophys* 45:RG2004.
23. Burbank DW, Beck RA, Mulder T (1996) *Asian Tectonics*, eds Y An and M Harrison (Cambridge University Press, Cambridge), pp 149–188.
24. Geddes A (1960) The alluvial morphology of the Indo-Gangetic Plains: its mapping and geographical significance. *T I Brit Geogr* 28:253–277.
25. Sinha R, Sarkar S (2009) Climate-induced variability in the Late Pleistocene-Holocene fluvial and fluvio-deltaic successions in the Ganga plains, India. *Geomorphology* 113:173–188.
26. *Geological Survey of Pakistan* (Government of Pakistan, Ministry of Industries and Natural Resources, Pakistan) Geological Map of Pakistan.
27. Schuldenrein J, Wright RP, Mughal R, Khan MA (2004) Landscapes, soils, and mound histories of the Upper Indus Valley, Pakistan: new insights on the Holocene environments near ancient Harappa. *J Archaeol Sci* 31:777–797.
28. Wright RP, Schuldenrein J, Mughal MR (2005) *South Asian Archaeology 2001*, eds C Jarrige and V Lefèvre (CNRS, Paris), pp 327–336.
29. Whipple KX, Parker G, Paola C (1998) Channel dynamics, sediment transport, and the slope of alluvial fans: experimental study. *J Geol* 106:677–693.
30. Leeder MR, Mack GH (2001) Lateral erosion ('toe-cutting') of alluvial fans by axial rivers: implications for basin analysis and architecture. *J Geol Soc London* 158:885–893.
31. Wobus CW, Tucker GE, Anderson RS (2010) Does climate change create distinctive patterns of landscape incision? *J Geophys Res* 115:F04008.
32. Clift PD, et al. (2012) U-Pb zircon dating evidence for a Pleistocene Sarasvati River and Capture of the Yamuna River. *Geology* 40:211–214.
33. Saini HS, Tandon SK, Mujtaba SAI, Pant NC, Khorana RK (2009) Reconstruction of buried channel-floodplain systems of the northwestern Haryana Plains and their relation to the 'Vedic' Saraswati. *Current Sci India* 97:1634–1643.
34. Gibling MR, Tandon SK, Sinha R, Jain M (2005) Discontinuity-bounded alluvial sequences of the southern Gangetic plains, India: aggradation and degradation in response to monsoonal strength. *J Sed Res* 75:369–385.
35. Makaske B (2001) Anastomosing rivers: a review of their classification, origin and sedimentary products. *Earth-Sci Rev* 53:149–196.
36. Lambrick HT (1964) *Sind: A General Introduction*, (Sindh Adabi Board, Pakistan), 1.
37. Harbor DJ, Schumm SA, Harvey MD (1994) *The Variability of Large Alluvial Rivers*, eds SA Schumm and B Winkley (American Society of Civil Engineers), 161–176.
38. Tremenheere CW (1867) On the lower portion of the River Indus. *J Roy Geog Soc* 37:68–91.
39. Holmes DA (1968) The recent history of the Indus. *Geogr J* 134:367–382.
40. Fleitmann D, et al. (2003) Holocene forcing of the Indian monsoon recorded in a stalagmite from southern Oman. *Science* 300:1737–1739.
41. Gupta AK, Anderson DM, Overpeck JT (2003) Abrupt changes in the Asian southwest monsoon during the Holocene and their links to the North Atlantic Ocean. *Nature* 421:354–356.
42. Herzschuh U (2006) Palaeo-moisture evolution in monsoonal Central Asia during the last 50,000 years. *Quaternary Sci Rev* 25:163–178.
43. Wulf H, Bookhagen B, Scherler D (2010) Seasonal precipitation gradients and their impact on erosion in the Northwest Himalaya. *Geomorphology* 118:13–21.
44. Chen F, et al. (2008) Holocene moisture evolution in arid central Asia and its out-of-phase relationship with Asian monsoon history. *Quaternary Sci Rev* 27:351–364.
45. Giosan L, et al. (2006) Recent morphodynamics of the Indus delta shore and shelf. *Cont Shelf Res* 26:1668–1684.
46. Clift P, et al. (2008) Holocene erosion of the Lesser Himalaya triggered by intensified summer monsoon. *Geology* 36:79–82.
47. Singh RN, et al. (2008) Settlements in context: reconnaissance in Western Uttar Pradesh and Haryana. *Man Environ* XXXIII:71–87.
48. Petrie CA, et al. (2009) Investigating changing settlement dynamics on the plains: the 2009 survey and excavations at Masudpur (Hissar District, Haryana). *Puratattva* 39:38–49.
49. Stein MA (1942) A survey of ancient sites along the 'Lost' Saraswati river. *Geogr J* 99:173–182.
50. Joshi RD, Madhu B, Jassu R (1984) *Frontiers of the Indus Civilization*, eds BB Lal and SP Gupta (Indian Archaeological Society jointly with Indian History & Culture Society, London).
51. Mallah Q (2008) *Linguistics, Archaeology and the Human Past, Occasional Paper 3*, eds T Osada and A Uesugi (Research Institute for Humanity and Nature, Nakanishi Printing Co Ltd, Kyoto), pp 27–76.
52. Flam L (1981) The paleogeography and prehistoric settlement patterns in Sind, Pakistan (~4000–2000 B. C.). Ph.D. thesis (Univ of Pennsylvania).
53. Enzel Y, et al. (1999) High-resolution Holocene environmental changes in the Thar Desert, northwestern India. *Science* 284:125–128.
54. Weiss H, et al. (1993) The genesis and collapse of third millennium North Mesopotamian civilization. *Science* 261:995–1004.
55. Hassan F (1997) *Third Millennium B.C. Climate Change and Old World Collapse*, eds HN Dalfes et al. (Springer, Berlin-Heidelberg-New York), pp 1–23.
56. Cullen HM, et al. (2000) Climate change and the collapse of the Akkadian empire: evidence from the deep sea. *Geology* 28:379–382.
57. Staubwasser M, Sirocko F, Grootes PM, Segl M (2003) Climate change the 4.2 ka BP termination of the Indus valley civilization and Holocene south Asian monsoon variability. *Geophys Res Lett* 30:1425, doi: 10.1029/2002GL016822.
58. Weber SA, Belcher WR (2003) *Indus Ethnobiology: New Perspectives from the Field* (Lexington Books, Lanham, MD).
59. Law RW (2008) *Occasional Paper 11: Linguistics, Archaeology and the Human Past* (Research Institute for Humanity and Nature, Nakanishi Printing Co. Ltd, Kyoto).
60. Goswami BN, Venugopal V, Sengupta D, Madhusoodanan MS, Xavier PK (2006) Increasing trend of extreme rain events over India in a warming environment. *Science* 314:1442–1445.

Supporting Information

Giosan et al. 10.1073/pnas.1112743109

SI Text

Geomorphic Mapping. The morphology of the Indo-Gangetic Plain was analyzed using high-resolution (90-m) digital elevation data derived from NASA's Shuttle Radar Topography Mission (SRTM; 1). Digital elevations models (DEMs) were constructed for the entire Indo-Gangetic Plain at 300 m resolution and at 200 and 100 m resolution for the Indus region. The DEMs were used in combination with Advanced Spaceborne Thermal Emission and Reflection Radiometer (ASTER) and Google Earth to identify geomorphic patterns that provide insight into fluvial morphodynamics. Large-scale (tens to hundreds of kilometers long) regional linear features with vertical morphological expression cutting across elevation contours were visually identified and interpreted with the aid of DEM cross-profiles and 3D navigation to map the extent and location of fluvial channels, ridges, terraces, and incised valleys. Locations of dried channels were verified using published morphological and geological data (2–6) as well as through our own field survey, trenching, and drilling in Pakistan.

Lithostratigraphy. The selection of sampling locations for sedimentary deposits (organized on transects in Figs. S1–S3; Fig. 2) was based on our geomorphic mapping as well as on published literature on the morphology (4–6) and geology (2, 3) of the western Indo-Gangetic Plain. Shallow sampling techniques included vibro- and percussion corings as well as manual and digger-aided trenching. Rotary drilling was employed at Matli and Nara in Sindh as well as Tilwalla and Marot in Cholistan (Punjab). At several locations in Punjab, Pakistan (Dipalpur, Karan Shah, Kalokay, and Doda) sampling was performed directly in large-scale exposures (i.e., hundreds to thousands of meters outcrop length) in sand quarries. Based on lithofacies characteristics (i.e., lithology, textures, structures, and bedding), we identified and logged aeolian sands, fluvial deposits, soils, and anthropogenic overburden. Older and thicker soils were encountered preferentially in Punjab and Sindh. Anthropogenic overburden (road fill) was present at Okara in Punjab. Logs are presented in Fig. S4. Aeolian deposits were sampled at several locations along the Nara-Hakra-Ghaggar transect in the Pat and Cholistan regions of Pakistan (Figs. S2 and S4), including Fakirabad, Yazman, and in dedicated dune trenches at locations MGJ-3 and MGJ-5. The aeolian lithofacies was characterized by clean siliciclastic, massive to cross-stratified aeolian deposits composed of moderate- to well-sorted fine to medium sands.

Fluvial deposits were sampled at all sites (except at dune locations) directly from the surface or below soils, aeolian sands, or anthropogenic fill. On the Sindh transect (Figs. S1 and S4), we targeted channel deposits along dried Indus distributary courses at Shah Dipalli as well as floodplain deposits immediately adjacent to Indus distributary channels at Mirwah, Matli, and Merkan. Channel deposits were composed dominantly of poorly sorted, fine to coarse siliciclastic sands, with massive to faint parallel bedding/lamination. Floodplain deposits are predominantly finer, with over bank interstratified muds (clays, silts) and poorly sorted fine to medium sands. Carbonate nodules are small and rare, indicating a slow pedogenesis in this region. Below floodplain deposits, at Mirwah we encountered *ca.* 3 m of massive poorly sorted fine to medium channel sands. The borehole at Matli penetrated similar floodplain (and possibly crevasse splay) and channel deposits down to 45 m, where it encountered thin limestone gravels over Eocene limestone. At all Sindh sites, biogenic remains were

rare, consisting primarily of freshwater bivalves and subordinately gastropods.

Along the Nara-Hakra-Ghaggar transect (Fig. S2), fluvial siliciclastic deposits consisting of overbank interstratified muds and sands and channel deposits were generally finer than in Sindh (Fig. S4), suggesting lower energy flows (except for specifically targeted higher energy depositional environments, such as the bar deposits at Nara Chenab and Fort Abbas). Carbonate nodules are common in the Cholistan (Bahawalpur) region, indicating a more intense paleo-pedogenesis. At Fort Abbas, channel and sandy islands/bars deposits were both sampled; their lithofacies are suggestive of alterations in flow frequency and magnitude. Channel deposits are characterized by alternating flat bedded sand units with thin discontinuous silts, some of which had been desiccated, broken up, and then incorporated in the overlying sand unit, with thicker silt units at top and base. Dominantly fine overbank mud sequences, sometimes overlying coarser channel deposits, were sampled at Fort Derawar, Yazman, Alkasur Cotton Jinner, Marot (S-1), and Fort Abbas (S-3), and from the Sutlej bank at SUT-2. Deposits recovered from boreholes at Nara, Tilwalla, and Marot consist of similar alternating sequences of overbank deposits and coarser channels deposits. At all drill sites on this transect, a coarsening downward trend into the Pleistocene deposits is evident. Biogenic remains at sites along the Nara-Hakra-Ghaggar transect were again rare, consisting primarily of plant/wood and gastropods remains.

In Punjab (Figs. S3 and S4), large-scale exposures in sand quarries allowed us to examine channel deposits in extensive outcrops. Deposits are systematically coarser than in Sindh or Cholistan, consisting primarily of braided channel deposits and scour fills; overbank deposits at the top were generally thinner than 2 m, consisted of undifferentiated muds, and were strongly modified by human activity and root bioturbation. Braided channel deposits are composed of fine to coarse sands with thin (decimeter scale) levels of matrix-supported to imbricated pebbles. Bedding is tabular to lenticular and laterally continuous over a 10 s to 100 s meters, and decimeters to a few m thick. Sedimentary structures include large (submeter thick) cross stratification, parallel or cross lamination in fine sands, channel scours (of meter size depth), and pebble imbrications indicative of channel lag deposits. Channel or bar deposits were also sampled in trenches at Okara (below overburden) and Jahanabad (below well-developed soil). Carbonate nodules were present at the top of all sites, indicating postdepositional pedogenesis. Biogenic remains at sites along the Punjab transect were rare and consisted primarily of charcoal and freshwater bivalves.

Chronology. Optically stimulated luminescence. At the Aberystwyth Luminescence Research Laboratory, all samples were prepared in subdued red light conditions. The 90–125 μm grain-size fraction was used for dating, after treatment with hydrochloric acid and hydrogen peroxide to remove carbonates and organic matter, respectively. Heavy liquid density separation ($2.62 < \rho < 2.70 \text{ g/cm}^3$) was carried out to isolate the quartz grains, and the resulting material was etched using hydrofluoric acid to remove the alpha-irradiated outer surface of the quartz grains and remove any nonquartz minerals still present. Optically stimulated luminescence (OSL) measurements were made using a Risø TL/OSL luminescence reader, and OSL was stimulated using blue light-emitting diodes ($470 \pm 20 \text{ nm}$). The resulting signal was measured through a bialkali photo multiplier tube fitted with 7.5 mm U340 filters. Equivalent dose (D_e) measurements were

made following the single-aliquot regenerative dose (SAR) protocol (7) on small aliquots [2 mm in diameter (8)] of sample, with a preheat of 220 °C for 10 s and a cut-heat of 160 °C for 0 s used during the measurement cycles. A standard set of rejection criteria (9) was applied, including the OSL IR depletion ratio of Duller (10) to check for signal contamination by feldspar. The protocol of Rodnight, et al. (11) was followed to decide whether to use the central age model or the finite mixture model (FMM) to calculate a D_e for age calculation (Table S1). The environmental dose rate to grains was calculated using a combination of thick source alpha and beta counting, to assess the impact of radioactivity resulting from the decay of uranium, thorium, and potassium. The environmental dose due to cosmic rays was calculated using the equations of Prescott and Hutton (12).

At the Royal Holloway, University of London Luminescence Laboratory, all samples were prepared in subdued red and amber light conditions. All grain-size fractions used for dating (chosen based on dominant grain-size in the sample; Table S2) were treated with hydrochloric acid and hydrogen peroxide to remove carbonates and organic matter, respectively. Heavy liquid density separation at 2.70 g cm⁻³ was carried out to remove heavy minerals. The 125–180 and 180–250 µm grain-size fractions were etched using hydrofluoric acid to remove the alpha-irradiated outer surface of the quartz grains and remove nonquartz minerals, while the 40–70 µm grain-size fraction of Okara was immersed in fluorosilicic acid for 2 weeks to remove nonquartz material. Multigrain (medium-size aliquots, ca. 5 mm) OSL measurements were made using a Risø TL-DA TL/OSL luminescence reader and OSL was stimulated using blue light-emitting diodes (470 ± 20 nm). The resulting signal was measured through 9235QA photo multiplier tube fitted with 6 mm of Hoya U340 filters. D_e measurements were made following the single-aliquot regenerative dose (SAR) protocol (7), with an initial preheat of 240 °C for 10 s and second preheat, following application of a test dose, of 200 °C for 10 s used during the measurement cycles. These values were selected after a preheat plateau dose recovery test was applied to Karan Shah and after testing on Okara and Jahanabad using a dose recovery test (13). A standard set of rejection criteria (9) were applied, including the OSL IR depletion ratio of Duller (10), to check for signal contamination by feldspar. The signal was integrated from the first 0.8 s of OSL decay minus a background between 3.2 and 6.4 s. The D_e used for age calculation was obtained from the weighted mean (Table S2). For Okara, an alpha efficiency value of 0.04 ± 0.02 was assumed (14).

Single-grain OSL measurements were conducted on samples where the grain-size used was 180–250 µm using a Risø TL-DA TL/OSL luminescence reader. OSL was induced using a green (532 nm) 10 mW Nd : YVO₄ laser focused on aluminum disks with 100 chambers with 300 µm by 300 µm dimensions. The resulting signal was measured through 9235QA photo multiplier tube fitted with 6 mm of Hoya U340 filters. D_e measurements were made following the SAR protocol (7), with an initial preheat of 240 °C for 10 s and a second preheat, following application of a test dose, of 200 °C for 10 s used during the measurement cycles. In addition to applying a standard set of rejection criteria (9) and OSL IR depletion ratio of Duller (10), grains were rejected if the uncertainty on the test dose was >20%. The signal was integrated from the 0.08–0.16 s of OSL stimulation, while background was subtracted from the last 0.17 s. In both cases the D_e used for age calculation was obtained from the central age model (CAM, 15). The CAM was chosen due to the relatively normal shape of the distribution of grain equivalent doses [the skewness parameter, c , was less than $2\sigma_c$, the significance of the skew value multiplied by 2 (16)].

Dose rates were calculated from uranium, thorium, and potassium contents measured using Inductively Coupled Plasma Mass Spectrometry (ICP-MS) and Atomic Emission Spectrometry (-AES). ICP samples were taken from the light-exposed ends

of sample tubes, with sediment being homogenized and subsampled for ICP analysis. Samples were prepared by lithium metaborate or sodium peroxide fusion. Given the arid climate of the region and the well-drained nature of the deposits, water contents during burial were assumed to be *ca.* 20% of the measured saturation value (Table S2). Alpha and beta attenuation was obtained using calculations in Bell (17) and Mejdahl (18), respectively, and dose-rate conversion factors were taken from Adamiec and Aitken (19). Uncertainties are based on the propagation, in quadrature, of individual errors for all measured quantities, which if unknown are taken as 10%. In addition to uncertainties calculated from counting statistics, errors due to (i) beta source calibration (3%; 20), (ii) radioisotope concentration (10%), (iii) dose-rate conversion factors (3%), and (iv) attenuation factors (3%) have been included (21). The cosmic dose was calculated using present-day burial depth (12).

Radiocarbon. Plant, wood, and charcoal remains as well as mollusk shell samples for ¹⁴C dating were collected from fluvial and aeolian deposits where available (Fig. S4). The depth of each sample was recorded relative to the local surface. All samples were cleaned ultrasonically and, for inorganic carbon samples, we removed the outer part of the shell via standard acid etching. Accelerator mass spectrometry (AMS) radiocarbon dating was performed at the National Ocean Sciences Accelerator Mass Spectrometry Facility (NOSAMS) at the Woods Hole Oceanographic Institution. The methodology for AMS radiocarbon dating is presented on the NOSAMS site (www.whoi.edu/nosams) and discussed in McNichol, et al. (22). All dates have been converted to calendar ages (2 sigma range) relative to 2010 using Calib 5.0.1 software (23) and the IntCal04 calibration dataset (24) and a 60-year positive correction. All radiocarbon dates and their calibrated equivalents together with the location information in core for the dated samples and their geographical location are presented in Table S3.

Archaeological Sites Distribution, Ages, and Patterns of the Harappan Collapse. The sources for archaeological site locations and their radiocarbon and/or archaeological ages are published gazetteers (25–30). Most of the sites were already consolidated in Gangal, et al. (31). To this database we added sites from gazetteers of Punjab (26, 27), Haryana (28), and Sindh (29) in Pakistan and several sites studied during the Harappa and Beas regional survey (32).

Site distribution provides an important line of evidence for social changes in the Late Harappan period and for characterizing urban collapse in this region. Compilations of site counts, and estimated site sizes, by period [e.g., Possehl (33)] indicates that the total settled area declines from approximately 7,358 to approximately 4,484 hectares [ha] during the transition to Post-Urban Harappan times. This area is calculated from the average site area, based on the estimates by Possehl, multiplied by the total number of sites. The average site size drops from 7.2 to 3.2 ha; the latter reflects the reduction of large cities like Harappa and Mohenjodaro to smaller occupied areas. Nevertheless, the total number of archaeological sites increased, from 1,022 to 1,281, which indicates that on average there were many more smaller sites. As discussed in our main text, there is also a significant shift in site numbers and density towards the east. Looking at particular regions, there is a particularly precipitous decrease in sites in Sindh, from around 90 sites to 19 (30, 33, 34). Meanwhile, in the Ghaggar-Hakra, differences are seen between the Cholistan (western) area and upper Ghaggar-Hakra (eastern) area (see Fig. 5 in ref. 31). The western area sees a decrease from 174 sites to 41 and an estimated settled area of 974 to 209 ha, while in the eastern area sites numbers increase from 218 to 853; despite this massive increase, however, estimated settled area only rises from 2,943 to 2,985 ha (34, 35). The latter estimates indicate clearly the fall in average site size. Decrease in the number of

sites occurred also in areas outside the core Harappan region on the Indo-Gangetic plain, such as Baluchistan and Gujarat (Fig. S5 and ref. 31). While more recent archaeological field surveys (28, 30, 32, 36, 37) will have added some site numbers, these do not affect the general patterns that have been evidenced for over a decade. These numbers can therefore be taken as indicative of the shifts that constitute urban collapse at the end of the Harappan civilization in terms of the distribution of human population. The changes in settlement size and the distribution of sites in relation to climate and landscape imply that adjustments might have been made to the agricultural subsistence base. To further illustrate these points graphically (Fig. S5), we use the Gangal, et al. database (31), updated as described above.

- Harappan Crop Compilation.** Changes in the commonness of Harappan crops over time were compiled by Fuller (38), based on 53 archaeological sites and/or cultural phases with published archaeobotanical evidence and excluding crops occurring in less than 15% of all sites or with uncertain specific identification (Fig. S6). These data included Harappan-era sites, with archaeobotanical evidence, from the Saurashtra peninsula. This evidence indicates a strategic shift in agricultural practices, with more sites practicing two seasons of cultivation. An increasing proportion of sites farmed summer crops, mainly reliant on monsoon rains, in the Post-Urban Harappan period. During the Early and Mature Harappan period, most of those sites with evidence for summer cereals (millets) are located in the eastern areas of the Harappan civilization.
1. Farr TG, et al. (2007) The Shuttle Radar Topography Mission. *Rev Geophys* 45: 10.1029/2005RG000183.
 2. Geological Survey of Pakistan (1964) *Geological Map of Pakistan* (Government of Pakistan, Ministry of Industries and Natural Resources).
 3. Kazmi AH (1984) *Marine Geology and Oceanography of Arabian Sea and Coastal Pakistan*, eds Haq BU, Milliman JD (Van Nostrand Reinhold, NY), pp 65–70.
 4. Holmes DA, Western S (1969) Soil texture patterns in the alluvium of the lower Indus plains. *J Soil Sc* 20:23–37.
 5. West Pakistan Water and Power Development Authority (1966) *Lower Indus Report: Hunting Technical Service* (M. MacDonald & Partners, Lahore).
 6. Holmes DA (1968) The recent history of the Indus. *Geograph J* 134:367–382.
 7. Murray AS, Wintle AG (2000) Luminescence dating of quartz using an improved single-aliquot regenerative-dose protocol. *Rad Measur* 32:57–72.
 8. Duller GAT (2008) Single-grain optical dating of Quaternary sediments: why aliquot size matters in luminescence dating. *Boreas* 37:589–612.
 9. Jacobs Z, Duller GAT, Wintle AG (2006) Interpretation of single grain De distributions and calculation of De. *Rad Measur* 41:264–277.
 10. Duller GAT (2003) Distinguishing quartz and feldspar in single grain luminescence measurements. *Rad Measur* 37:161–165.
 11. Rodnight H, Duller GAT, Wintle AG, Tooth S (2006) Assessing the reproducibility and accuracy of optical dating of fluvial deposits. *Quat Geochron* 1:109–120.
 12. Prescott JR, Hutton JT (1994) Cosmic ray contributions to dose rates for luminescence and ESR dating: large depths and long-term time variations. *Rad Measur* 23:497–500.
 13. Murray AS, Wintle AG (2003) The single-aliquot regenerative dose protocol: potential improvements in reliability. *Rad Measur* 37:377–381.
 14. Rees-Jones J (1995) Optical dating of young sediments using fine-grain quartz. *Ancient TL* 13:9–13.
 15. Galbraith RF, Roberts RG, Laslett GM, Yoshida H, Olley JM (1999) Optical dating of single and multiple grains of quartz from Jinmium rock shelter, northern Australia: Part I, Experimental design and statistical models. *Archaeometry* 41:339–364.
 16. Bailey RM, Arnold LJ (2006) Statistical modelling of single-grain quartz De distributions and an assessment of procedures for estimating burial dose. *Quat Sci Rev* 25:2475–2502.
 17. Bell WT (1980) Alpha dose attenuation in quartz grains for thermoluminescence dating. *Ancient TL* 12:4–8.
 18. Mejndahl V (1979) Thermoluminescence dating: beta-dose attenuation in quartz grains. *Archaeometry* 21:61–72.
 19. Adamiec G, Aitken MJ (1998) Dose rate conversion factors: update. *Ancient TL* 16:37–50.
 20. Armitage SJ, Bailey RM (2005) The measured dependence of laboratory beta dose rates on sample grain size. *Rad Measur* 39:123–127.
 21. Murray AS, Olley JM (2002) Precision and accuracy in the optically stimulated luminescence dating of sedimentary quartz: a status review. *Geochronometria* 21:1–16.
 22. McNichol AP, et al. (1995) Improvements in procedural blanks at NOSAMS: Reflections of improvements in sample preparation and accelerator operation. *Radiocarbon* 37:683–691.
 23. Stuiver M, et al. (1998) INTCAL98 Radiocarbon age calibration. *Radiocarbon* 40:1041–1083.
 24. Reimer PJ, et al. (2004) IntCal04 terrestrial radiocarbon age calibration, 0–26 cal kyr BP. *Radiocarbon* 46:1029–1058.
 25. Joshi RD, Madhu B, Jassu R (1984) *Frontiers of the Indus Civilization*, ed Lal BB (Books & Books, India).
 26. Mughal MR (1996) *Pakistan Archaeology* Vol. 29, eds Iqbal F, Khan MA, Hassan M (Department of Archaeology and Museums, Pakistan; Karachi).
 27. Mughal MR (1997) *Ancient Cholistan: Archaeology and Architecture* (Ferozsons Press, Karachi, Pakistan).
 28. Kumar M (2009) *Linguistics, Archaeology and the Human Past, Occasional Paper* 7, eds Osada T, Uesugi A (Research Institute for Humanity and Nature, Nakanishi Printing Co. Ltd., Kyoto), pp. 1–75.
 29. Possehl GL (1999) *Indus Age. The Beginnings* (University of Pennsylvania Press, Philadelphia).
 30. Mallah QH (2010) *Current Studies on the Indus Civilization Rohn-Manohar Indus Project Series*, eds Osada T, Uesugi A (Manohar Publishers, India), pp 27–76.
 31. Gangal K, Vahia M, Adhikari R (2010) Spatio-temporal analysis of the Indus urbanization. *Current Sci* 98:846–852.
 32. Wright RP, Schuhdenrein J, Mughal MR (2005) *South Asian Archaeology 2001*, eds Jarrige C, Lefèvre V (CNRs, Paris), pp. 327–36.
 33. Possehl GL (1997) The transformation of the Indus Civilization. *Journal of World Prehistory* 11:425–472.
 34. Possehl GL (1999) Prehistoric population and settlement in Sindh in *The Indus River: Biodiversity, Resources, Humankind*, eds. Meadows A, Meadows PS (Oxford University Press, Pakistan).
 35. Possehl GL (2000) In *The drying up of the Sarasvati: environmental disruption in South Asian prehistory. Environmental Disaster and the Archaeology of Human Response*, eds Bawden G, Reycraft M. (Maxwell Museum of Anthropology, University of New Mexico, Albuquerque, NM) Papers no. 7.
 36. Singh RN, et al. (2008) Settlements in context: reconnaissance in Western Uttar Pradesh and Haryana. *Man Environ* XXXIII:71–87.
 37. Petrie CA, et al. (2009) Investigating changing settlement dynamics on the Plains: the 2009 survey and excavations at Masudpur (Hissar District, Haryana). *Puratattva* 39:38–49.
 38. Fuller DQ (2011) Finding plant domestication in the Indian subcontinent. *Curr Anthropol* 52:S347–S362.

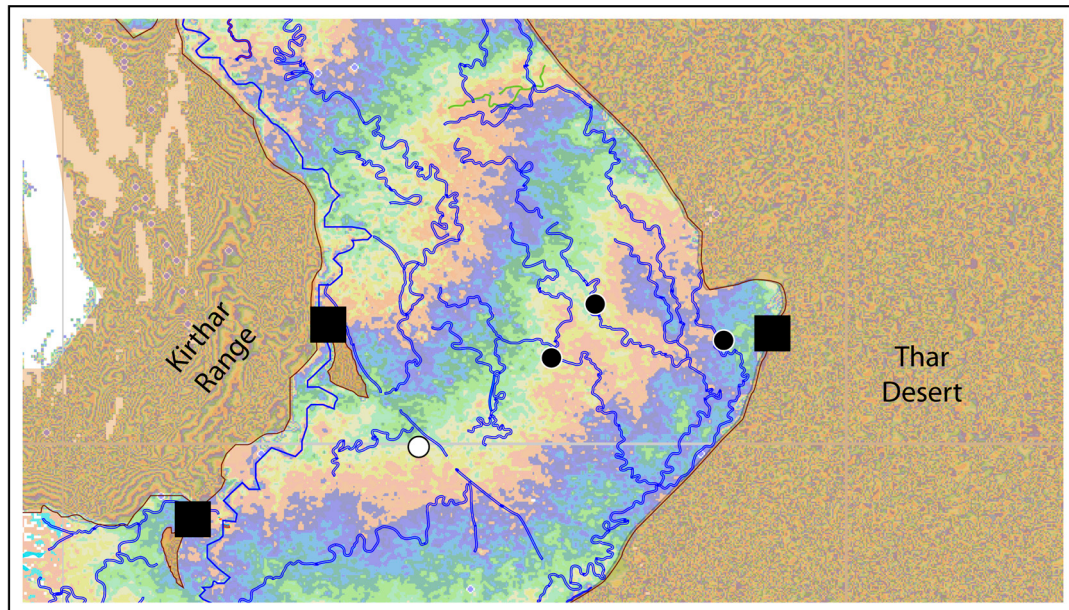
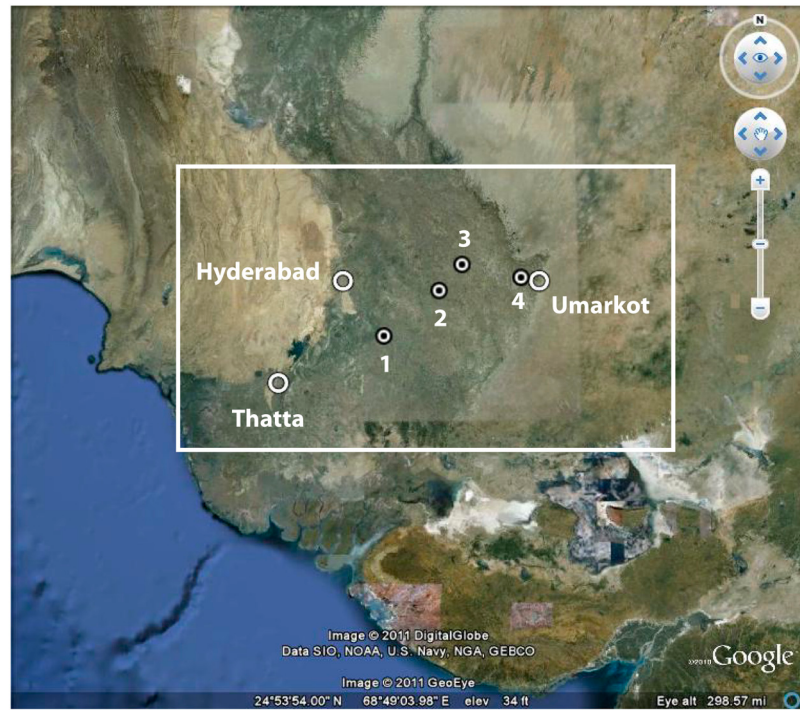


Fig. S1. Upper: Location of sampling sites in lower Sindh on a Google Earth image of the Indus alluvial plain and delta: 1 = Matli; 2 = Mirwah; 3 = Shah Dipalli; 4 = Merkan; the modern city of Hyderabad and towns of Thatta and Umarkot are also identified. The white box shows the extent of the region shown in lower box. Lower: SRTM-derived DEM with interpreted distributary channel courses, locations of sampling sites, and localities identified in upper box. Drill sites are represented by white circles, and shallow sampling sites are depicted by black circles. For altitudes, pattern of colors repeats every 10 m. Nonalluvial or desert regions are covered by a transparent brown mask.

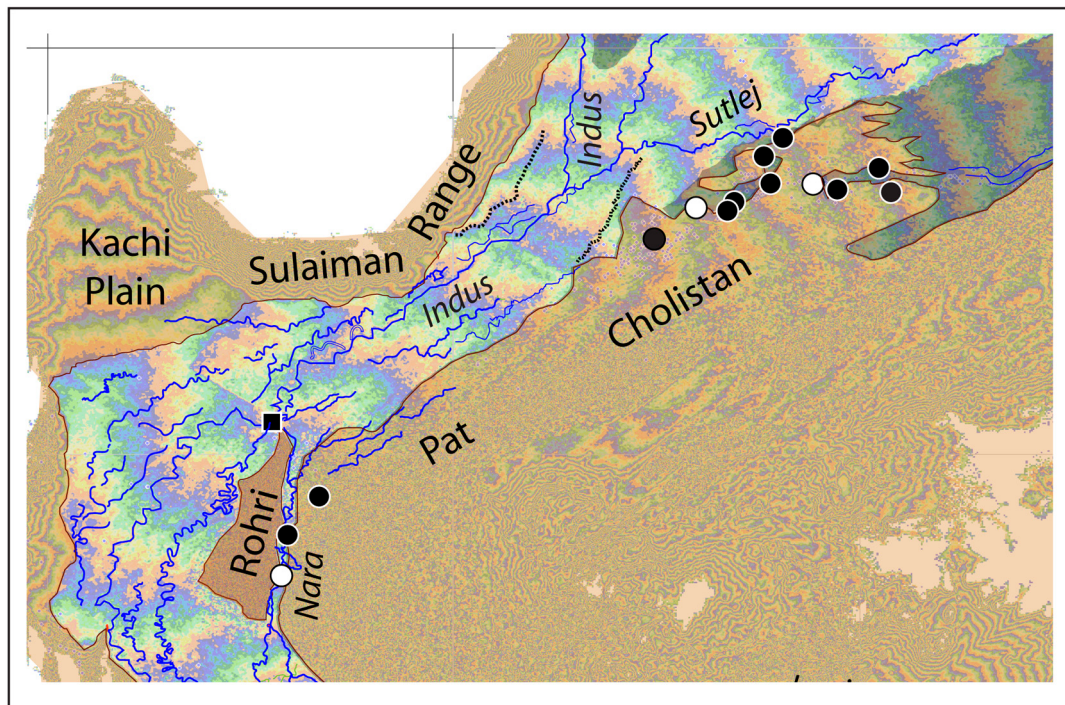
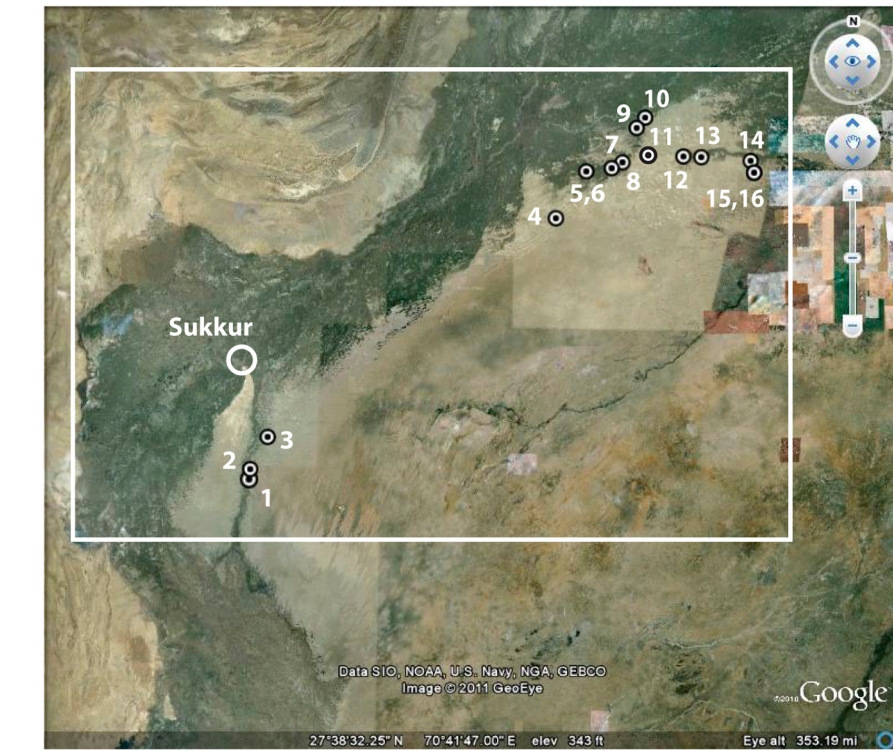


Fig. S2. Upper: Location of sampling sites in Pat region and Cholistan (Bahawalpur region) on a Google Earth image of the Indus and Nara-Ghaggar-Hakra alluvial plains: 1 = Fakirabad; 2 = Nara Kenab; 3 = Nara; 4 = Ft.Derawar; 5 = Basti; 6 = Tilwalla; 7 = Yazman; 8 = Alkasur Cotton Jinner; 9 = SUT-2; 10 = MGJ-5; 11 = Marot; 12 = Marot (1); 13 = Ft.Abbas (3); 14 = Ft.Abbas (MGJ-2); and 15 = Ft.Abbas (MGJ-1); the modern city of Sukkur is also identified. The white box shows the extent of the region shown in lower box. Lower: SRTM-derived DEM with interpreted distributary channel courses, locations of sampling sites, and localities identified in upper box. Black dotted lines show terrace edges. Drill sites are represented by white circles, and shallow sampling sites are depicted by black circles. For altitudes, pattern of colors repeats every 10 m. Nonalluvial or desert regions are covered by a transparent brown mask.

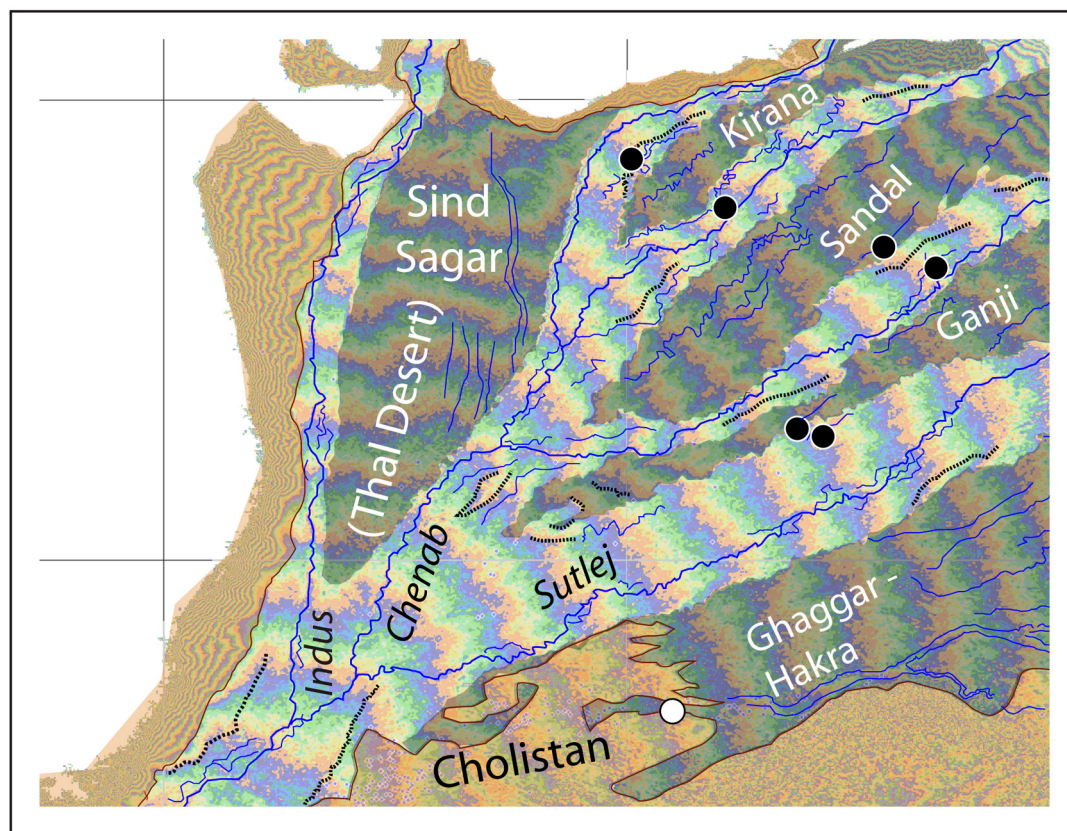
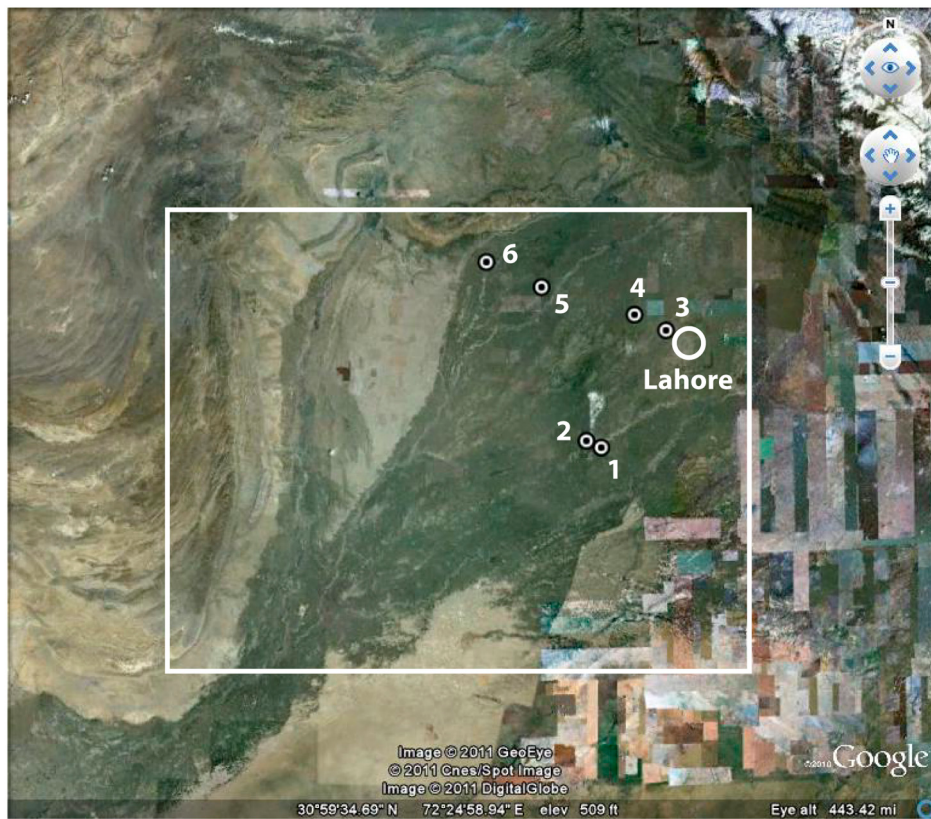


Fig. S3. Upper: Location of sampling sites in Punjab, Pakistan on a Google Earth image of the combined alluvial plain of the Indus and Punjab rivers: 1 = Dipalpur; 2 = Okara; 3 = Karan Shah; 4 = Kalokay; 5 = Doda; 6 = Jahanabad; the modern city of Lahore is also identified. The white box shows the extent of the region shown in lower box. Lower: SRTM-derived DEM with interpreted distributary channel courses, locations of sampling sites (black circles), and localities identified in upper box. For altitudes, pattern of colors repeats every 10 m. A gray mask identifies interfluves. Nonalluvial or desert regions are covered by a transparent brown mask.

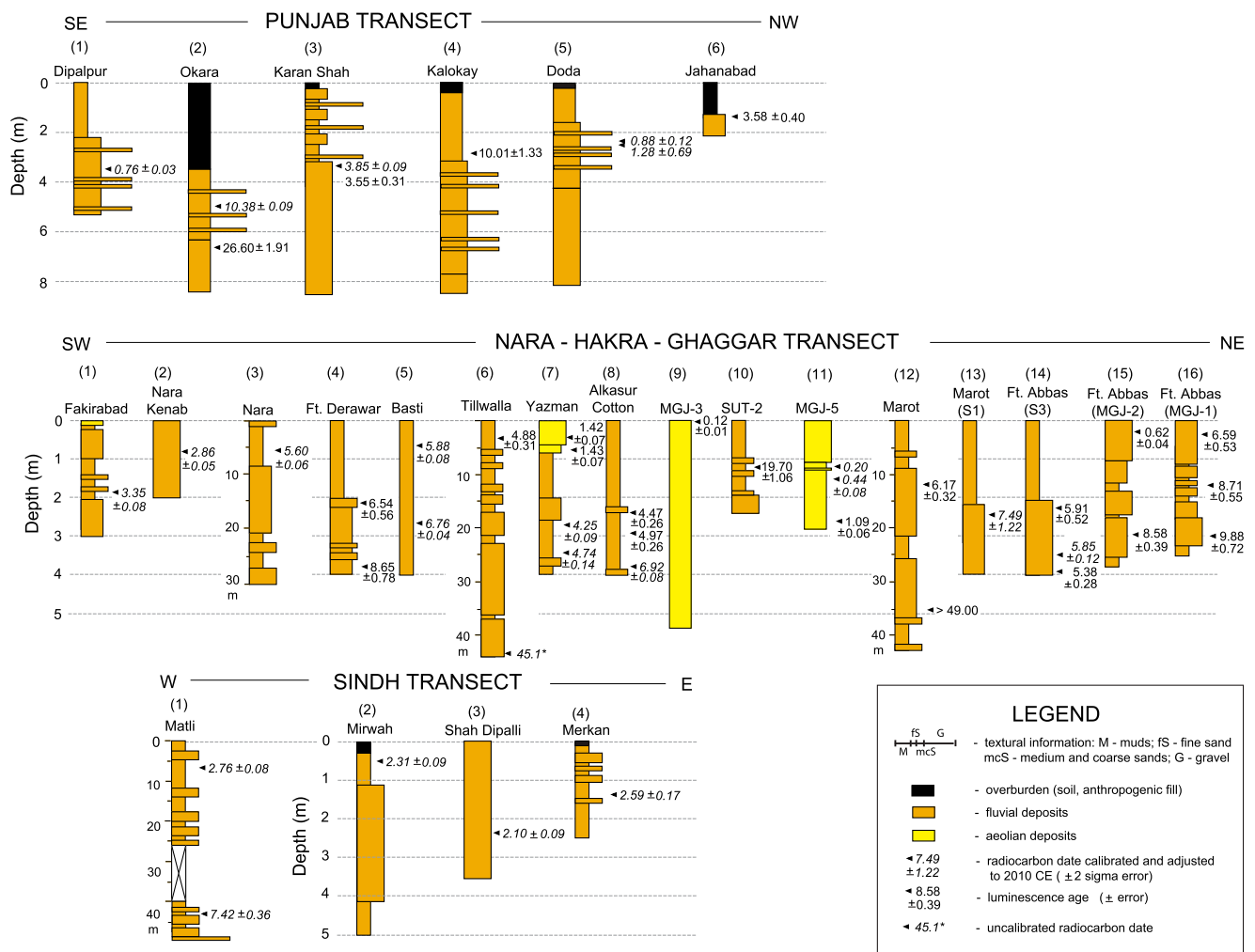


Fig. S4. Core logs and their OSL and radiocarbon chronology for sites examined in the Indo-Gangetic Plain along three transects in Pakistan. Geographical location of numbered sites on each transect are identified visually in Figs. S1–S3 and numerically in Tables S1–S3.

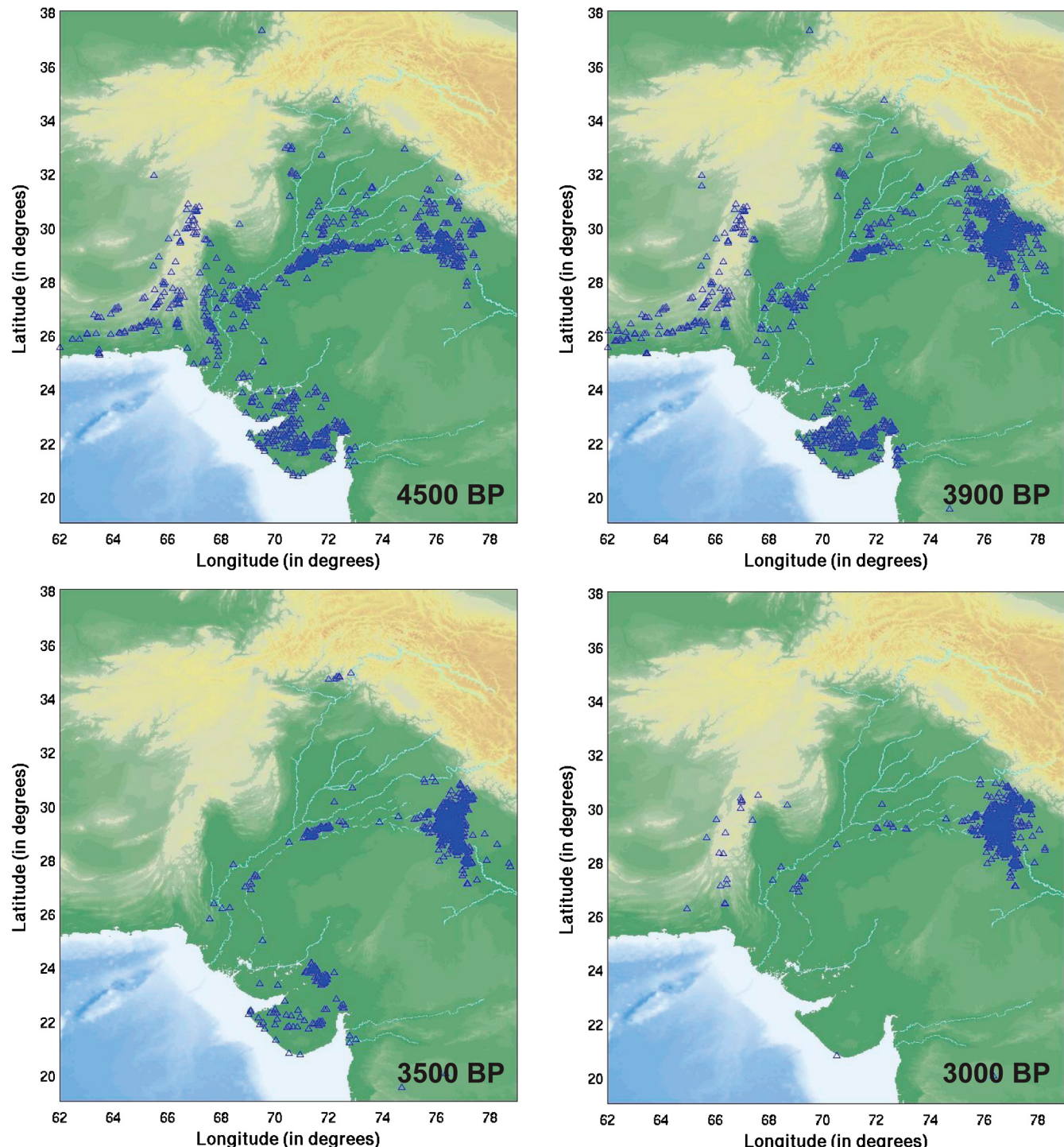


Fig. 55. Distribution of archaeological sites in the Indus domain approximately 4,500, 3,900, 3,500, and 3,000 y ago (updated with data from ref. 31, 26–29, 32).

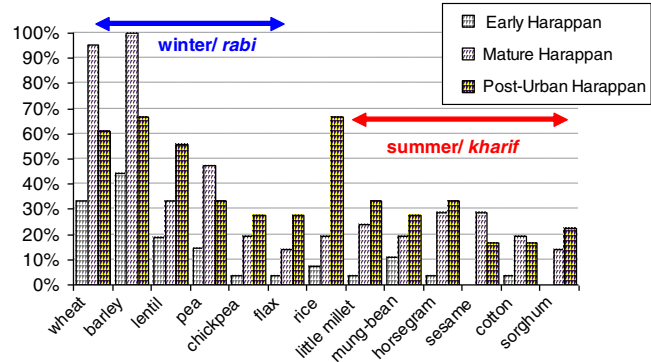


Fig. S6. Changes in the commonness of crops in the Harappan civilization over time, comparing winter/spring grown (*Rabi*) crops (dependent largely on riverine water sources) and summer grown (*Kharif*) crops (dependent largely on monsoon rains). Note the general increase from Early, Mature, to Post-Urban for summer crops, while winter crops became less common in the Post-Urban period.

Table S1. OSL age analytical data from Aberystwyth Luminescence Research Laboratory

No.	Location	Sample code	Depth (m)	Aliquots*	H_2O (%)	σ_d^t	Age model ^t	Infinite-dose-rate (Gy/kyr) ^s			Cosmic dose-rate (Gy/kyr) ^s	Total dose-rate (Gy/kyr) ^s	Age (kyr ago) ^s
								Equivalent dose (Gy) ^s	matrix beta dose-rate (Gy/kyr) ^s	Gamma dose-rate (Gy/kyr) ^s			
4	Fort Derawar	Aber/136-S6-1	2.08	108 (36)	5 ± 2	0.34	MAM	22.9 ± 1.75	2.40 ± 0.08	1.50 ± 0.10	0.16 ± 0.02	3.64 ± 0.13	6.54 ± 0.56
4	Fort Derawar	Aber/136-S6-7	3.81	108 (28)	5 ± 2	0.26	MAM	26.5 ± 2.20	1.95 ± 0.06	1.40 ± 0.10	0.13 ± 0.01	3.06 ± 0.10	8.65 ± 0.78
6	Tiwalla	Aber/TIL3-2	3.69–3.72	72 (36)	25 ± 5	0.46	FMM	13.6 ± 0.57	2.33 ± 0.08	1.48 ± 0.10	0.13 ± 0.01	2.91 ± 0.14	4.88 ± 0.31
7	Yazman	Aber/154-MGJ-6-2	0.95	72 (39)	5 ± 2	0.28	FMM	4.34 ± 0.14	1.95 ± 0.06	1.25 ± 0.08	0.18 ± 0.02	3.08 ± 0.11	1.43 ± 0.07
7	Yazman	Aber/154-MGJ-6-3	1.25	108 (29)	5 ± 2	0.37	FMM	4.84 ± 0.16	2.20 ± 0.07	1.43 ± 0.09	0.17 ± 0.02	3.42 ± 0.13	1.42 ± 0.07
8	Alkasur Cotton Jinner	Aber/136-S4-1	2.32	60 (26)	5 ± 2	0.21	CAM	14.4 ± 0.64	2.07 ± 0.07	1.36 ± 0.10	0.15 ± 0.02	3.22 ± 0.12	4.47 ± 0.26
8	Alkasur Cotton Jinner	Aber/136-S4-2	2.91	107 (54)	5 ± 2	0.52	FMM	19.3 ± 0.67	2.51 ± 0.08	1.67 ± 0.12	0.14 ± 0.01	3.88 ± 0.15	4.97 ± 0.26
9	MGJ-3	Aber/154-MGJ-3-6	0	72 (28)	5 ± 2	0.79	FMM	0.37 ± 0.03	1.96 ± 0.06	1.26 ± 0.09	0.28 ± 0.03	3.16 ± 0.12	0.12 ± 0.01
10	SJT-2-1	Aber/155-SUT-2-1	2.2	84 (23)	5 ± 2	0.28	FMM	60.7 ± 2.40	2.05 ± 0.07	1.31 ± 0.09	0.15 ± 0.02	3.08 ± 0.11	19.7 ± 1.06
11	MGJ-5	Aber/154-MGJ-5-5	2.25	96 (26)	5 ± 2	0.2	CAM	3.25 ± 0.14	1.92 ± 0.06	1.26 ± 0.09	0.15 ± 0.01	2.99 ± 0.11	1.09 ± 0.06
12	Marot	Aber/153-MAR2-5B	10.86–10.92	48 (43)	25 ± 5	0.11	CAM	23.9 ± 0.46	3.24 ± 0.10	1.95 ± 0.13	0.06 ± 0.01	3.87 ± 0.19	6.17 ± 0.32
12	Marot	Aber/153-MAR2-13B	34.32–34.38	96 (34)	25 ± 5	-	>140	2.25 ± 0.07	1.62 ± 0.13	0.01 ± 0.01	2.84 ± 0.15	>49 ^t	5.91 ± 0.52
14	Ft. Abbas (S3)	Aber/136-S3-1	2.22	60 (23)	5 ± 2	0.19	CAM	17.8 ± 1.38	1.87 ± 0.06	1.36 ± 0.10	0.15 ± 0.02	3.01 ± 0.13	5.38 ± 0.28
14	Ft. Abbas (S3)	Aber/136-S3-9	3.99	96 (46)	5 ± 2	0.23	CAM	15.1 ± 0.54	1.81 ± 0.06	1.19 ± 0.08	0.13 ± 0.01	2.81 ± 0.11	5.38 ± 0.28
15	Ft. Abbas (MGJ-2)	Aber/154-MGJ-2-1	0.3	96 (35)	5 ± 2	0.42	FMM	2.07 ± 0.11	2.08 ± 0.07	1.42 ± 0.10	0.22 ± 0.02	3.33 ± 0.12	0.62 ± 0.04
15	Ft. Abbas (MGJ-2)	Aber/154-MGJ-2-5	3.25	96 (28)	5 ± 2	0.28	FMM	25.8 ± 0.64	1.91 ± 0.06	1.32 ± 0.10	0.14 ± 0.01	3.01 ± 0.12	8.58 ± 0.39
16	Ft. Abbas (MGJ-1)	Aber/154-MGJ-1-1	0.67	48 (22)	5 ± 2	0.25	FMM	22.3 ± 1.39	2.17 ± 0.07	1.40 ± 0.16	0.19 ± 0.02	3.38 ± 0.17	6.59 ± 0.53
16	Ft. Abbas (MGJ-1)	Aber/154-MGJ-1-4	1.57	126 (28)	5 ± 2	0.32	CAM	27.1 ± 1.72	1.77 ± 0.06	1.12 ± 0.08	0.17 ± 0.02	2.74 ± 0.10	9.88 ± 0.72
16	Ft. Abbas (MGJ-1)	Aber/154-MGJ-1-8	2.9	60 (31)	5 ± 2	0.27	CAM	25.2 ± 1.29	1.82 ± 0.06	1.25 ± 0.09	0.14 ± 0.01	2.89 ± 0.11	8.71 ± 0.55

The geographical location of dated sites is shown in Fig. S2 and dated sample locations within each section are shown in Fig. S4.

*The number of aliquots measured is shown, with the number of aliquots passing all rejection criteria (and used in age calculation) shown in parentheses.

^t σ_d refers to the overdispersion parameter of Galbraith, et al. (1) used to assess the dose distribution.^sGalbraith RM, Green PF (1990) Estimating the component ages in a finite mixture. *Nuclear Tracks and Radiation Measurements* 17:197–206.[†]CAM refers to the central age model, and FMM to the finite mixture model [Galbraith, et al. (1)].[‡]Galbraith RM, Green PF (1990) Estimating the component ages in a finite mixture. *Nuclear Tracks and Radiation Measurements* 17:197–206.

§The equivalent doses, dose rates, and ages are shown to three significant figures. All calculations were made prior to rounding.

¶The luminescence signal of sample at the base of Marot is saturated. Therefore, a minimum age is given.

Table S2. OSL age analytical data from Royal Holloway Luminescence Lab

Location	Depth (m)	Grain-size (μm)	H_2O content (%) [*]	σ_d^{\dagger}	SG CAM equivalent dose (Gy) [#]	MG equivalent dose (Gy) [#]	Alpha dose-rate (Gy kyr^{-1}) ^{\$}	Infinite-matrix beta dose-rate (Gy kyr^{-1}) ^{\$}	Cosmic dose-rate (Gy kyr^{-1}) ^{\$}	Total dose-rate (Gy kyr^{-1}) ^{\$}	SG CAM Age (kyr) ["]	MG Age (kyr) ["]
Okara	2.6	40–73	7.5 ± 1	n/a	n/a	76.7 ± 3.37 (15)	0.30 ± 0.12	1.26 ± 0.08	0.14 ± 0.01	2.88 ± 0.16	n/a	26.6 ± 1.91
Karan Shah	3.5	180–250	6.6 ± 1	0.3	9.21 ± 0.66 (46)	9.20 ± 0.65 (15)	n/a	1.38 ± 0.11	0.13 ± 0.01	2.60 ± 0.13	3.55 ± 0.31	3.54 ± 0.31
Kalokay	3.1	180–250	5.1 ± 1	0.7	26.5 ± 3.26 (39)	30.4 ± 2.98 (10)	n/a	1.41 ± 0.11	1.10 ± 0.07	0.14 ± 0.01	2.65 ± 0.13	10.0 ± 1.33
Jahanabad	1.0	125–180	5.9 ± 1	n/a	n/a	10.1 ± 0.86 (15)	1.47 ± 0.11	1.16 ± 0.06	0.18 ± 0.02	2.81 ± 0.14	n/a	3.58 ± 0.35

The geographical location of dated sites is shown in Fig. S3, and dated sample locations within each section are shown in Fig. S4.

*Water contents taken as 20% of saturation value ±10%.

[†] σ_d refers to the overdispersion parameter of Galbraith, et al. (2) used to assess the dose distribution.

[#]Galbraith RM, Green PF (1990) Estimating the component ages in a finite mixture. *Nuclear Tracks and Radiation Measurements* 17:197–206.

^{\$}The equivalent dose are shown to three significant figures with number of aliquots used in parentheses. All calculations were made prior to rounding. SG CAM = single grain using central age model; MG = multigrain (medium-size aliquots, approximately 5 mm).

^{\$}Dose rates are shown to three significant figures. All calculations were made prior to rounding.

["]Ages are shown to three significant figures. All calculations were made prior to rounding. SG CAM = single grain using central age model; MG = multigrain (medium-size aliquots, approximately 5 mm).

Table S3. Results of AMS ^{14}C dating of organic materials recovered from locations shown in Figs. S1–S3

Location	Depth (m)	Latitude (deg min)	Longitude (deg min)	Type	^{14}C Age (yr BP)	Error (yr)	Cal. age (yrs)*	Cal. age (yrs)*	Error (yrs)	Sedimentation rates (m/kyr)	Number [‡]
<i>Punjab transect</i>											
Dipalpur	3.50	30 43.962	73 35.351	charcoal	760	30	667–730	759	32		1
Okara	5.00	30 47.226	73 27.099	bivalve	9,150	35	10,233–10,407	10,380	87		2
Karan Shah	3.30	31 39.636	74 12.169	bivalve	3,520	30	3,701–3,875	3,848	87		3
Doda	2.50	32 00.573	73 02.415	gastropod	860	35	690–904	875	125		5
Doda	2.60	32 00.573	73 02.415	charcoal	1,280	30	1,149–1,288	1,279	70		5
<i>Nara—Hakra—Ghaggar transect</i>											
Nara	0.80	26 54.371	68 59.119	bivalve	2,670	25	2,747–2,844	2,856	49		1
Kenab											
Nara	6.00	26 58.561	68 59.474	bivalve	4,830	25	5,481–5,607	5,604	63		2
Fakirabad	1.85	27 12.224	69 07.174	gastropod	3,080	35	3,215–3,373BP	3,354	79		3
Basti	0.75	29 11.236	72 15.028	gastropod	5,050	20	5,740–5,893	5,877	77		5
Basti	2.65	29 11.236	72 15.028	gastropod	5,880	20	6,659–6,743	6,761	42		5
Tilwalla	43.7	29 05.740	71 34.084	plant/wood	45,100	670					6
Yazman	2.70	29 07.386	71 46.168	gastropod	3,810	20	4,097–4,283	4,250	93		7
Yazman	3.55	29 07.386	71 46.168	gastropod	4,130	20	4,540–4,815	4,738	138		7
Alkasur	3.81	29 09.907	71 51.325	gastropod	6,010	50	6,787–6,928	6,918	71		8
Cotton											
Jinner											
MGJ-5	1.10	29 10.082	72 01.148	plant/wood	145	25	modern–282	201	141		11
MGJ-5	1.40	29 10.082	72 01.148	plant/wood	315	30	303–464	444	81		11
Marot (S1)	2.40	29 12.816	72 20.475	gastropod	6,500	50	7,308–7,552	7,490	122		13
Ft. Abbas (S3)	3.45	29 11.409	72 52.909	gastropod	5,050	35	5,668–5,906	5,847	119		14
Ft. Abbas (MGJ-1)	2.59	29 06.450	72 54.542	gastropod	11,900	50	13,708–13,961	13,835	127	†	16
Ft. Abbas (MGJ-1)	2.96	29 06.450	72 54.542	gastropod	12,000	70	13,785–14,077	13,931	146	†	16
<i>Sindh transect</i>											
Matli	6.7	25 02.670	68 39.309	bivalve	2,610	30	2,624–2,776	2,760	76	2.4	1
Matli	40.2	25 02.670	68 39.309	plant/wood	6,520	180	7,000–7,716	7,418	358	7.2	1
Mirwah	0.5	25 19.589	69 02.512	bivalve	2,250	25	2,158–2,340	2,309	91	0.2	2
Shah	2.3	25 29.336	69 12.215	bivalve	2,070	35	1,947–2,133	2,100	93	1.1	3
Dipalli											
Merkan	1.35	25 24.514	69 35.425	bivalve	2,430	30	2,353–2,698	2,586	173	0.5	4

Sample locations within each section are shown in Fig. S4.

*Calendar ages are relative to year 2010.

[†]Ages on mollusk fragments; probably reworked; not used in age models.

[‡]Number refers to lithostratigraphic log for sample in Fig. S4.